8-2019

Ipsc Based Gene Correction And Disease Model Of A New Class Of Lgmd Due To Poglut1 Mutation

Jose Ortiz-Vitali

IPSC BASED GENE CORRECTION AND DISEASE MODELING OF A NEW CLASS OF LGMD DUE TO POGLUT1 MUTATION

A

THESIS

Presented to the Faculty of

The University of Texas

MD Anderson Cancer Center UTHealth

Graduate School of Biomedical Sciences

In Partial Fulfillment

of the Requirements

for the Degree of

MASTER OF SCIENCE

by

Jose Ortiz-Vitali, B.S.

Houston, Texas

August 2019

Dedicated to my mother and father for their unending love, support, and sacrifice in pushing me to be the person I am today

Acknowledgments

I would like to express my gratitude towards Dr. Darabi for giving me the opportunity to lead this project and be a part of his laboratory. From the beginning he has shown me nothing but kindness and understanding throughout my journey at IMM. Even at my darkest and most challenging times he led me with patience and never drove me to question my abilities, and in fact reassured them and urged me to work diligently through the problems that I faced. It has been an incredibly rewarding experience being a part of his team.

I would also like to thank Dr. Jianbo Wu who has been my teacher at the lab bench every day since I started this journey. While Dr. Darabi has fundamentally and conceptually led me from start to finish in this research project, Dr. Wu has taught me day-to-day the procedures at the lab bench that have helped me hone my skills as scientist into what they are today. Without him I would not have a wide array of skills that will follow me throughout my career. I cannot even begin to count the amount of times I have asked him the simplest to the most complex of questions, and he always had the time to sit with me and explain over and over if needed until I understood the concept or work I was doing. I am forever indebted to the knowledge he has imparted with me.

And to the others in my laboratory who have helped me immensely, Sean and Liang. Though our time as lab mates is brief, the impact is deep. We have had many meaningful conversations and pondered the science in our hands numerous times and I will always cherish the time spent during the days at IMM. When results were negative, we always built each other up because we know that the best science is built on failure.

And thank you to the others in the center for the time we've shared on breaks for lunch, coffee, or just to talk and avoid our work just because we can. You know who you are.

To my family here in Houston, the love I have for each one of you is never ending and each of you has a role in this journey. Thank you to my father and mother for supporting me every step of the way, and for being there for me to unconditionally love and care for me. For providing a roof over my head while I struggle during this journey, to preparing food for me to take with me on long nights. For understanding the times that I would come home late from experiments that took far too much time to complete, and not asking any questions when I have zero energy to even carry a conversation and just disappear into my room for the night. This degree is as much yours as it is mine.

And last but certainly not least, Sabrina. Thank you for your endless support in the final year of this degree and for always pushing me to stay strong when things just wouldn't go my way. You've seen me shed tears over this work, and you've spent dozens of hours in the laboratory sleeping and waiting for me to finish. Those hours were definitely not the ideal way to spend a Friday or Saturday night, but you understood and supported me with minimal complaint because you knew it had to be done. I will always appreciate that, and this is for you too.

IPSC BASED GENE CORRECTION AND DISEASE MODELING OF A NEW CLASS OF LGMD DUE TO POGLUT1 MUTATION

Jose Ortiz-Vitali, B.S.

Advisory Professor: Radbod Darabi, PhD

Recently, a novel class of muscular dystrophy has been discovered in a family due to autosomal recessive missense mutation in POGLUT1. Mutation of this enzyme leads to decreased O-glucosyltransferase activity and impaired Notch signaling, the pathways important for skeletal muscle stem cell (satellite cells) quiescence and activation. We hypothesize that reduced POGLUT1 activity and impaired Notch signaling is causative of this limb girdle muscular dystrophy through dysfunction of muscle stem cells and myogenic progenitors.

To test this, we have used iPSCs for disease modeling and rescue experiments. Using a CRISPR based gene targeting method, we aimed to correct the point mutation and restore POGLUT1 function, thus restoring Notch signaling activity. Following correction, iPSC-derived gene corrected myogenic cells were differentiated and compared to healthy control and patient cell line (isogenic control). Compared to patient cells, gene-corrected cells demonstrated superior ability to proliferate and improved myogenic potential as compared to patient uncorrected cells. In addition, Notch signaling pathway activity was improved in the corrected cells as a result of the POGULT1 gene correction. These results support our hypothesis that POGULT1 modulates Notch signaling in myogenic cells and its involvement may be responsible for the development of this type of LGMD.

TABLE OF CONTENTS

LIST OF TABLES

LIST OF FIGURES

ABBREVIATIONS

ADAM	A disintegrin and metalloproteinase
BMD	Becker muscular dystrophy
BMP	Bone morphogenetic protein
BSA	Bovine serum albumin
BP	Base pair
cDNA	Complementary DNA
Cas9	CRISPR associated protein
CM	Conditioned media
CRISPR	Clustered regularly interspersed short palindromic repeats
CTL	Control
DAPI	4’,6’diamidino-2-phenylindole
DSB	Double strand break
DLL	Delta-like ligand
DMD	Duchenne muscular dystrophy
DM	Myotonic dystrophy
ECM	Extracellular matrix
EGF	Epidermal growth factor
FGF	Fibroblast growth factor
FSHD	Facioscapulohumeral muscular dystrophy
GAPDH	Glyceraldehyde 3-phosphate dehydrogenase
HGF	Hepatocyte growth factor
HDR	Homology directed repair

hESC	Human embryonic stem cell
HS	Horse Serum
IGF	Insulin growth factor
Indel	insertion deletion
iPSC	Induced pluripotent stem cell
KB	Kilobase pair
LGMD	Limb girdle muscular dystrophy
MDM-I	Myogenic differentiation medium stage 1
MDM-II	Myogenic differentiation medium stage 2
MDM-III	Myogenic differentiation medium stage 3
MEF	Mouse embryonic fibroblast
mRNA	Messenger RNA
NECD	Notch extracellular domain
NHEJ	Non-homologous end joining
NICD	Notch intracellular domain
POGLUT1	Protein *O*-glucosyltransferase 1
PT	Patient
PTC	Patient corrected
qPCR	Quantitative PCR
RIPA	Radioimmunoprecipitation assay buffer
ROCK	Rho-associated protein kinase
RT	Room temperature
TAE	Tris-acetate-edta

TGF-β	Transforming growth factor beta
WT	Wild-type

CHAPTER 1: INTRODUCTION

1.1Skeletal Muscle

Skeletal muscle makes up about a third or more of the human body's total mass, and its generation and regulation is a highly controlled step-wise process from embyrogenesis to post-natal myogenesis and onwards into adulthood. From the three germ layers that are formed in the embryo (ectoderm, endoderm, and mesoderm) the mesoderm and subsequently the paraxial (also known as pre-somitic or somitic) mesoderm gives rise to the sublayer that forms the skeletal muscle. Following specification of the sublayers of the mesoderm in early embryogenesis, a collection of signals from the dorsal ectoderm, neural tube, and notochord drive somitogenesis and the generation of myogenic precursors (Zhao & Hoffman, 2004). Somitic specification gives rise to the dermomyotome generating precursor cells expressing the transcription factors PAX3 and PAX7, which regulate early skeletal muscle formation, and post-natal growth and regeneration respectively (Relaix, et al., 2006). Committed myogenic progenitors expressing MYF5 enter the cell cycle and proliferate where they give rise to further committed $MYOD^{+}$ cells that exit the cell cycle eventually forming myoblasts that fuse and form $MYOG^{+}/MHC^{+}$ myotubes (Cusella-De Angelis, et al., 1992).

1.2 Satellite Cells: The Stem Cells of the Muscle

Within the highly organized skeletal muscle system there lies a system of maintenance and regeneration by stem cells to repair damaged fibers while also replenishing the pool of progenitors that give rise to the mature muscle. These cells

are known as satellite cells; quiescent stem cells lying just beneath the basal lamina of the myofiber which, upon injury, are activated and enter the cell cycle where it asymmetrically, and symmetrically (Le Grand, Jones, Seale, Scimè, & Rudnicki, 2009)divides to restore their own pool of satellite cells or give rise to $Pax7^{+}$ myogenic progenitors that repair the damaged muscle (MAURO, 1961), (Schultz, E., Gibson,M.C., Champion, 1978), (Zammit, et al., 2004). Expression of Pax7 is necessary for of myogenic specification and quiescence of satellite cells (Seale, et al., 2000). While both PAX3 and PAX7 define myogenic progenitors, MYF5, MYOD, MYOG, AND Desmin play an epistatic relationship to further drive terminal differentiation of myoblasts (Rudnicki et al. 1993), (Kassar-Duchossoy, 2004).

1.2.1 Satellite Cells in Maintenance and Recovery

The process by which the myofiber is damaged and undergoes necrosis, followed by activation, proliferation and differentiation of satellite cells ultimately ending in new myofiber formation is known as muscle regeneration. Studies have shown that targeted ablation of the satellite cell pool leads to lack of muscle regeneration (Lepper, Partridge, & Fan, 2011), (Sambasivan, et al., 2011) further corroborating the idea that this pool of satellite cells is critical for regeneration in adulthood regardless of physiological or pathological injury. In the events following muscle injury, satellite cells undergo a process of activation of the skeletal muscle program, and an upregulation of myogenic genes desmin, MyoD, myf5, and myogenin are observed, though proliferation of satellite cells is not seen until after 24 hours (Rantanen,Hurme, T., Lukka, R., Heino, J., Kalimo, 1995), (Cornelison & Wold,

1997). Fundamental work in discovering the regenerative capacity of satellite cells has shown that transplantation of single muscle fibers into radiation-ablated muscle can generate numerous new myofibers containing thousands of nuclei. These satellite cells are seen to proliferate and regenerate as well as self-renew (Collins, et al., 2005).

1.2.2 Signaling Pathways Governing Satellite Cell Renewal and Commitment

To drive regeneration, the satellite cells asymmetric and symmetric division is dependent on two key pathways: Notch and Wnt signaling. Symmetric distribution is driven through activation of planar cell polarity through Wnt7a activation of Vang12 through Frizzled (Le Grand, Jones, Seale, Scimè, & Rudnicki, 2009). In asymmetric division, the Notch pathway is involved. Notch signaling maintains quiescence in satellite cells and its downregulation allows for committed progenitors to differentiate. Notch signaling in muscle development and regeneration involves a complex interplay of ligands and receptors the likes of which still requires full elucidation, however many groups have begun to shed light on the combinatory functions of these signaling molecules. Notch signaling molecules includes expression of four receptors, Notch 1-4, and five canonical ligands DLL1, 3, and 4, and Jagged -1 and -2. Notch 1 and 2 in satellite cells has been shown by conditional knockouts to coordinate to regulate satellite cell function in the quiescent and activated state. Interestingly, single knockout of Notch 1 and 2, and double knockout showed no significant, slight reduction, and almost complete depletion of satellite cells in quiescence respectively. However, in the activated state, single knockouts of both

Notch 1 and 2 showed defect in regeneration and double knockout exhibited severe compromise of regeneration of the satellite cell pool. This shows Notch 1 and 2 must work synergistically to maintain the stem cell pool in quiescence (Fujimaki et al. 2017). Transplantation experiments showed that satellite cells expressed high levels of Notch3, whereas committed progenitors showed high levels of DLL1. Interestingly, Notch3 deficient showed hyperplasia after repeated muscle injury and may act as a negative feedback regulator of Notch signaling by repressing Notch 1 (Kitamoto et al. 2010). In primary myoblasts, low levels of DLL1 existed in $Myf5^-$ cells, but $Myf5^+$ cells exhibited high DLL1 levels. Upon inhibition of Notch signaling via DAPT (a γ-secretase inhibitor essential for proper Notch signaling), loss of the $Pax7^+/Myf5^-$ satellite cell pool was seen showing Notch signaling plays a key role of regulating self-renewal (Kuang, Kuroda, Le Grand, & Rudnicki, 2007).

1.3 Genetic Muscular Dystrophies

As stated previously, in normal adults' muscle regenerates following injury or stress. However, there exists a category of muscle disorders known as muscular dystrophies. These are rare genetic diseases that affect the skeletal muscle of the body and are characterized by progressive muscle damage, and invasion of fatty and fibrotic tissue within the muscle fibers, usually resulting in poor prognosis. There are currently dozens of identified muscle disorders ranging from mutations in key structural proteins of the muscle, signaling molecules, enzymes, and even errors in post-translational modification.

1.3.1 DMD and Other Common MDs

Of the 30 known types of muscular dystrophies, there are a handful that are more prevalent than others. Duchenne Muscular Dystrophy, and its milder form Becker Muscular Dystrophy, are the most common and well known. DMD affects 1 out of 3500 boys and is caused by a lack of dystrophin protein in the muscle achieved through X-linked recessive mutation (reduced expression of dystrophin is the cause of the milder form BMD) (Koenig, Monaco, & Kunkel, 1988). Dystrophin is expressed at the sarcolemma and binds at the DAPC to help link the ECM and cytoskeleton (Ervasti, Ohlendieck, Kahl, Gaver, & Campbell, 1990), (Yoshida & Ozawa, 1990). Loss of dystrophin leads to progressive muscle wasting early in age, and eventual death during or before teens by either cardiac or pulmonary failure. Another common type of muscular dystrophy is Myotonic dystrophy, the most common type of adult MD. DM is caused by an autosomal dominant mutation that leads to excessive CTG repeats in the 3' UTR (Mahadevan, et al., 1992). A unique type of MD known as FSHD differs from the usual disruption of gene function in that a loss of a subset of repeats in the D4Z4 macrosatellite repeat array of chromosome 4 does not disrupt structure of any particular gene (TYLER & STEPHENS, 1950), (Tawil & Van Der Maarel, 2006). Interestingly, a majority of FSHD cases experience *de novo* mutations (Tawil & Van Der Maarel, 2006). Lastly, there is a heterogeneous group of MD that has a wide range of types and causes known as limb girdle muscular dystrophy (LGMD). This MD is characterized by progressive muscle wasting beginning in mid-to-late teens and confining the patient to wheelchair later in adult life. Proximal

muscles of the body such as those attached to the trunk of the body as well as back and shoulders are most affected. Mutations in various components of the muscle such as Lamin A/C, Caveolin-3, α-dystroglycan, and glucosyltransferases all lead to various forms of LGMD which vary in severity (Galbiati et al. 2000), (Muchir, et al., 2000), (Brown, et al., 2004), (Servián-Morilla, et al., 2016).

1.3.2 Satellite Cell Function in Muscular Dystrophies

With the regenerative function of satellite cells in muscle, one can come to the conclusion that in DMD and other dystrophic patients, there must be a compensatory mechanism and exhaustion of the satellite cell pool from repeated injury and stress on muscles. In the mouse model for DMD (known as *mdx*) muscle degeneration in early age activates satellite cells which results in increased proliferation (Boldrin, Zammit, & Morgan, 2015) and with age, as well as disease progression, satellite cell self-renewal is decreased. Interestingly, a group using a Notch-reporter mouse has found that *mdx* satellite cells exhibit reduced activation of Notch signaling, which is necessary to maintain satellite cell quiescence and self-renewal, with constitutive Notch activation rescuing the self-renewal deficiencies (Kuang, Kuroda, Le Grand, & Rudnicki, 2007). This further implies that Notch signaling is essential for maintaining the satellite cell pool.

1.4 Discovery of LGMD2Z

Recently, collaborators in Spain have discovered a novel form of LGMD referred to as LGMD2Z. This disease arose in a consanguineous family where four out of five of the siblings in the family harbor a homozygous recessive missense mutation in a glucosyltransferase enzyme dubbed POGLUT1 (or *Rumi* in D. melanogaster) due to a c.699 T>G transversion, which led to a change in codon sequence from aspartic acid to glutamic acid at residue 233 (p.D233E). This enzyme is involved in Notch signaling post-translational modification and function. Patient muscles show reduced Notch signaling activity, decreased satellite cell pools, and hypo-glycosylation α-dystroglycan (Servián-Morilla, et al., 2016). Patient-derived myoblasts also showed decreased proliferation, aberrant differentiation, and overall decreased pool of $Pax7^{+}$ cells. Due to the decreased satellite cell pool and disrupted differentiation, it is believed that pathology is driven through Notch-dependent loss of satellite cells (Servián-Morilla, et al., 2016).

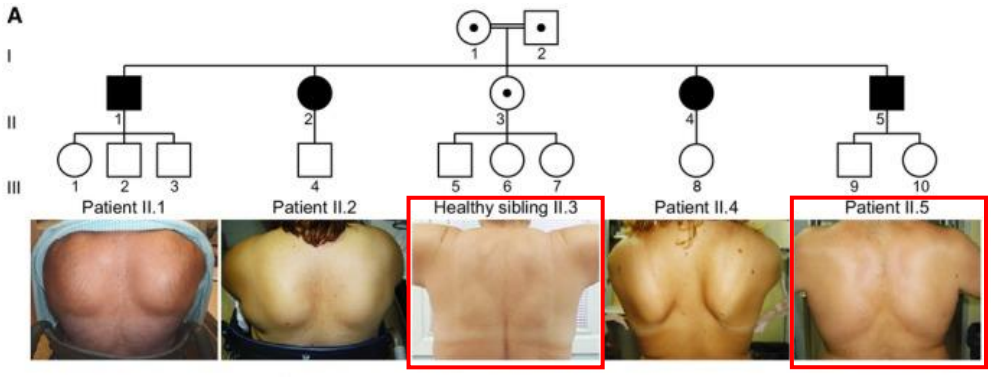

Figure 1 Family Pedigree Showing POGLUT1 Missense Mutation: Three out of five family members harbor the homozygous recessive missense mutation in POGLUT1. Characteristic of LGMD is winging of scapula seen in patients 1, 2, 4, and 5.

1.4.1 Notch Signaling and Satellite Cell Depletion in LGMD2Z

In the Notch signaling pathway, neighboring cells communicate via exchange through the Notch intracellular and extracellular transmembrane which facilitates cell-to-cell contact. Interactions with ligands leads to a series of proteolytic cleavage carried out by ADAM for the NECD and γ-secretase for release of the NICD from the cytosolic side of the membrane. Following cleavage, the NICD translocates to the nucleus where it complexes with binding proteins and transcriptional coactivators to activate expression of Notch target genes (such as the HES family of proteins (Kopan & Ilagan, 2009). Within the NECD lies a series of EGF repeats that contain a consensus sequence CXSX(P/A)C (Rana, et al., 2011). It is within these EGF repeats that post-translational modification of the NECD occurs. The NECD is modified with *O*-fucose and *O*-glucose glycans depending on the context in a tissue-specific manner and, if altered, affects Notch signaling. POGLUT1 plays a role in Notch signaling by adding *O*-glucose repeats to serine residues within the EGF repeats of the NECD. This post-translational modification is responsible for the NICD cleavage event by γ-secretase and improper cleavage leads to reduced Notch signaling activity (Acar, et al., 2008). POGLUT1 knockdown in mouse C2C12 cells has shown a decrease in *O*-glucosyltransferase activity and impaired Notch signaling (Fernandez-Valdivia, et al., 2011). As a result of decreased Notch signaling, proper activation of Pax7 does not occur, leading to progressive wasting of the satellite cell pool. Treating C2C12 cells with DAPT also shows decreased levels of Pax7 mRNA,

which is also seen in the muscles of patients. Interestingly, this wasting of the satellite cell pool does not occur immediately, but progressively, and patients have lived into early adulthood before disease progression becomes severe, ultimately confining them to wheelchair and severely limiting the use of the proximal muscles of the body (Servián-Morilla, et al., 2016). This is due to the otherwise normal development of the satellite cell pool, and a compensatory mechanism of regeneration of the limited pool before depletion.

1.5 Objectives and Hypothesis

We hypothesize that the POGLUT1 D233E missense mutation is causative of LGMD2Z affecting the Notch pathway to the extent of causing reduced Notch signaling, expansion, and self-renewal of satellite cells/myogenic progenitor cells and accelerated differentiation to myofibers.

1.5.1 Specific Aim I: CRISPR/Cas9n Based Gene Correction of POGLUT1 Mutation in Patient-Derived iPSCs:

A pair of site specific Cas9n gRNA constructs targeting the mutation region of POGLUT1 were delivered via electroporation along with a targeting construct containing two homology arms for POGLUT1 flanking a T2A-RFP-PURO selection cassette to generate DSB and facilitate HDR. This targeting construct contained loxP sites for removal of the selection cassette following selection and validation. Correction was verified via PCR analysis and DNA sequencing.

1.5.2 Specific Aim II: In Vitro Disease Modeling of Gene Corrected and Patient-Derived iPSCs:

Following validation of correction, control (CTL), patient (PT) and patient-corrected (PTC) cell lines underwent a directed differentiation protocol developed by our lab to validate reversal of pathology. This protocol recapitulates skeletal muscle myogenesis by driving cells towards PSM lineage followed by activation of dermomyotomal muscle progenitor cells. Validation of reversal of pathology will assist in further elucidating the role of POGLUT1 in Notch signaling.

CHAPTER 2: MATERIALS AND METHODS

2.1 Generation of iPSC line from Patient with LGMD2Z

Generation of LGMD2Z cell line is previously published data from the laboratory and referenced in the bibliography (Wu, et al., 2017).

2.2 Generation of Targeting Construct

Dr. Jianbo Wu of our laboratory previously generated the gRNA targeting sites for generation of DSB. *In silico* multiple possible target sites were generated and tested by SURVEYOR assay to determine %indel formation to estimate cutting efficiency. For construction of the targeting vector, the 3' end of the POGLUT1 homology arm was cut out of the pStartK backbone construct (Figure 1) which contained a 5' and 3' homology arm using restriction endonucleases NEB EagI-HF (Catalog #R3505S) and EcoRI-HF (Catalog #3101S) with NEB CutSmart® buffer (Catalog #B7204S) digested at 37°C for 3 hours. The 3' fragment of the POGLUT1 homology arm was then PCR amplified with conditions: initial denaturation at 95°C for 3 minutes; followed by 40 cycles of 95°C for 30 seconds, 62°C for 30 seconds, and 72°C for 1 minute followed by a final extension at 72°C for 10 minutes. PCR products were verified using 1% TAE agarose gel electrophoresis, ran for 30 minutes at 120V, and then purified using the Promega Wizard® SV Gel and PCR Clean-Up kit (Catalog #A9280). Once removed, the pStartK backbone that that had been cut was also purified using the Promega Wizard® SV Gel and PCR Clean-Up kit. Similarly, the selection cassette containing EF1 driven RFP T2A and Puromycin resistance was cut out of a pcDNA3.1 backbone (Figure 1) using NEB

Not1-HF (Catalog #3189S) and EcoR1-HF (Catalog #3101S) with NEB CutSmart® buffer (Catalog #B7204S) digested at 37°C for 3 hours.

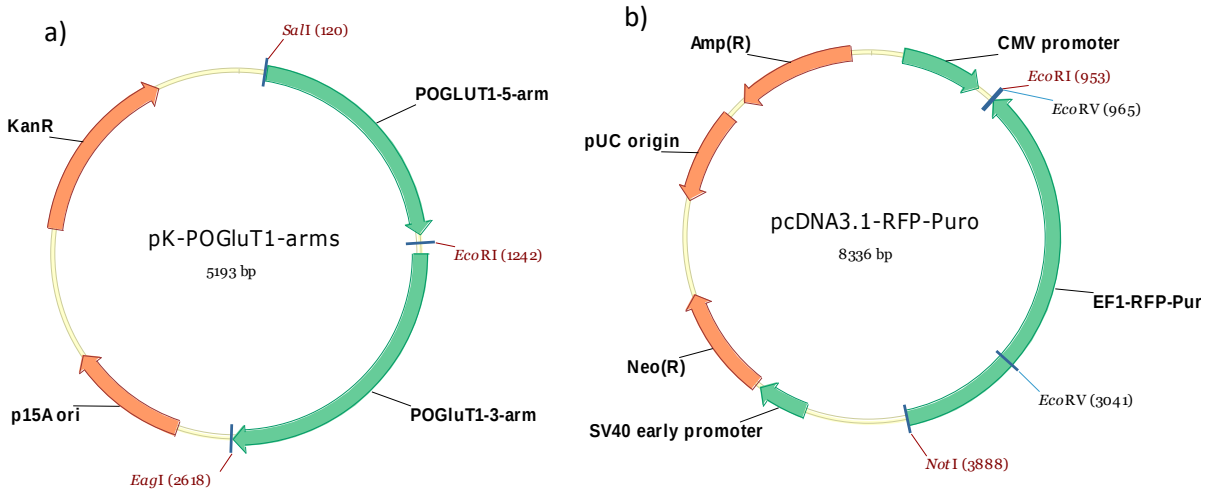

Figure 2 Tageting Construct Vectors: a) pStartK backbone containing POGLUT1 5' and 3' homology arms with unique EagI and EcoR1 sites to remove 3' arm. **b)** pcDNA3.1 backbone containing EF1-RFP-T2A-Puromycin selection cassette and specific cutting sites Not1 and EcoR1 for removal of the selection cassette.

The puromycin selection cassette purified from the pcDNA3.1 backbone and pStartK backbone containing only the 5' POGLUT1 homology arm were then ligated using the NEB NEBuilder® HiFi DNA Assembly Kit (Catalog #E5520S) as per the kit's instructions. To verify correct ligation of the pStartK backbone with 5' homology arm and puromycin resistance cassette, the construct was digested with NEB RsrII (Catalog #0501S) and CutSmart® buffer (Catalog #B7204S) digested at 37°C for 1 hour. Digested products were visualized on a 1% TAE agarose gel and ran for 30 minutes at 120V. Expected band sizes include 4.0kb, 1.5kb, and 1.1kb (Figure in results). Following verification of correct ligation, the construct was cut with Not1-HF (Catalog #3189S) to open for ligation. The purified 3' homology arm was then ligated back into the construct using NEB Gibson Assembly® kit (Catalog #E5510S) as per kit instructions. To verify correct insertion of 3' POGLUT1 homology arm, the construct was digested with NEB HindIII (Catalog #0104S) for 1 hour at 37°C. Digested product was then visualized using a 1% agarose gel ran for 30 minutes at 37°C. Expected bands were: 4.5kb, 2.3kb, and 1.6kb (Figure in results). Lastly, to generate the final construct to be used for targeting, a Gateway® cloning reaction using Thermo Fisher Gateway® LR Clonase® II (Catalog #1179120) was performed to transfer the construct from a pStartK backbone to pWS-TK6. Following Gateway® reaction, the reaction was transformed into One Shot® OmniMAX™ 2 $T1^R$ chemically competent E. coli. Cells were incubated on ice for 30 minutes, heat shocked for 30 seconds at 42°C, and placed on ice for 2 minutes. Cells were recovered with pre-warmed SOC broth and expanded for 1 hour at 37°C in shaking

incubator at 200rpm. Bacteria was then seeded onto ampicillin plates and grown overnight at 37°C. Final Construct is as seen in Figure 3.

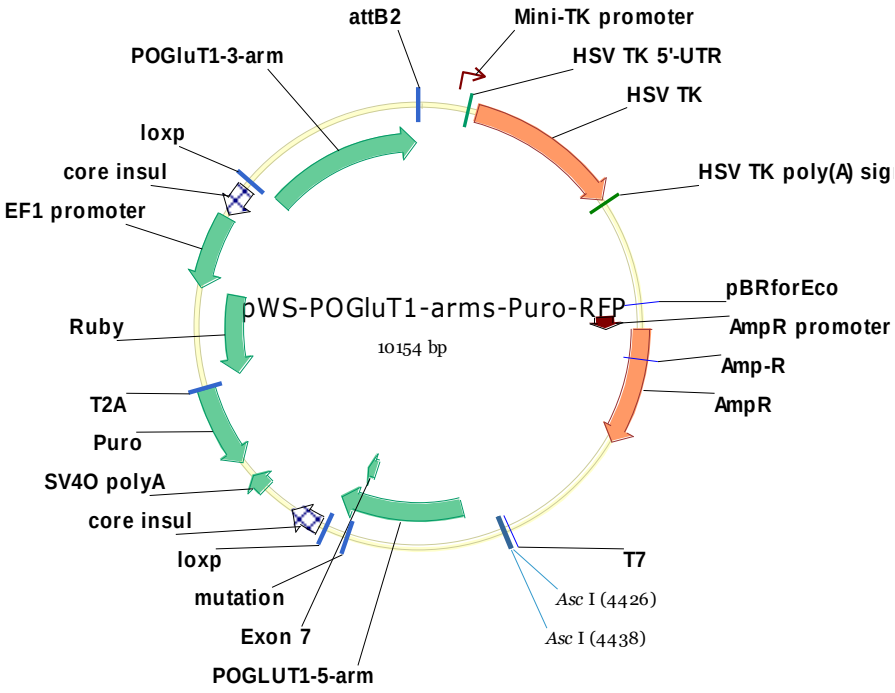

Figure 3 Map of Final Targeting Construct:

Map features include 5' and 3' POGLUT1 homology arms, puromycin selection cassette with EF1 promoter and T2A linking RFP Ruby and Puromycin resistance all flanked by loxP sites for removal after selection and HSV TK resistance for negative selection.

2.3 Electroporation of Cas9n Pair and pWS-POGLUT1-TK6-Puro construct

To prepare PT II.5 cells for electroporation, cells were grown in mTeSR™1 medium (Stem Cell Technologies, Catalog #85850) until 75% confluent and switched to MEF conditioned hES cell medium for two days supplemented with hr-FGF prior to electroporation: DMEM/F12 w/ GlutaMAX™ (Gibco, Catalog#10565018), 20% KSR™ (Gibco, Catalog #10828028), 1% MEM NEAA (Gibco, Catalog #11140050), 0.18% BME (Gibco, Catalog #21985023), 1% PS (Gibco, Catalog #15140122), 20ng/ml hr-FGF (Pepro Tech Inc, Catalog #100-18B). Once cells reached 60-80% confluency, cells were detached using ACCUTASE™ cell detachment solution (Stem Cell Technologies, Catalog #07920), pelleted at 200xg for 5 min, washed with PBS, and re-suspended in 100ul Lonza P3 Primary Cell 4D-Nucleofector™ solution containing 4µg of each construct (pWS targeting construct and two Cas9n sgRNA constructs) for nucleofection in the Lonza 4D-Nucleofector™ X unit (Lonza, Catalog #4VXP-3032). Cells were electroporated according to protocol CA139. Cells were recovered in complete hES medium and seeded onto gelatin coated dishes with B6 Puromycin resistant MEF cells (Gibco, Catalog #A34965) supplemented with ROCK inhibitor Y27632 (Millipore Sigma, Catalog #Y0503). Cells were allowed to recover until large noticeable colonies were formed from single cells and then treated with Puromycin to select for positive clones.

2.4 Expansion and validation of single-cell derived iPSC Clones

Following selection, puromycin treatment continued for ten days until colonies grew visibly once again to a large round shape and were picked. Picking colonies involved physical removal by creating grid pattern on the clone with 18g needle and removal with pipette. 30 colonies were seeded onto Corning Matrigel (Catalog #356234) coated plates with mTeSR™1 medium supplemented with Y27632. Cells were spun at 500 x g for 30 minutes at RT to promote attachment and increase survival of single-cell derived clones. Once picked colonies recovered, puromycin treatment was started again and maintained until cells were verified and frozen for stock. gDNA was extracted from picked clones using Lucigen QuickExtract™ DNA extraction Solution as suggested by protocol. gDNA extracted was used for PCR screen of primers (Table 1) amplifying the 5' and 3' regions of the POGLUT1 gDNA and spanning the selection insert. Primers (Table 1) to detect the wild type POGLUT1 without presence of the selection cassette was used as well for control. Clones picked that were screened positive were sent for DNA sequencing at LSLabs in the Texas Medical Center using reverse primer (Table 1) of 5' POGLUT1 homology arm which contains the region of the correction. Sequencing results analyzed using Chromas software. Following expansion of clones, puromycin selection cassette was removed by electroporation of 4µg Cre recombinase plasmid pCAG-Cre-IRES2-GFP (Addgene, Catalog #26646). Lonza 4D nucleofector P3 Kit as described before. Clones were seeded and expanded on multiple Corning matrigel (Catalog #356234) coated 96 well plates and allowed to recover with mTeSR™ Plus (Stem Cell Technologies, Catalog #05825) supplemented with CloneR™(Stem Cell Technologies, Catalog #05889) to increase survival of single-cell derived colonies. Once single-cell derived clones were identified, clones were expanded to larger wells while screening with primers specific to

loxP sites and POGLUT1 sequence (Table 1). Following expansion of PTC clones verified for correct removal of puromycin selection cassette, positive clone was stained for iPSC markers using Stemlight™ iPSC Reprogramming Antibody Kit (Stemlight™, Catalog #9092S) as per kit instructions.

Oligo Name	Sequence 5' to 3'
POGLUT1-783Mut-F	TGACCTGAACAACATACCCTTCA
POGLUT1-783Mut-R	GCTAATGCTGGTTCATGGAACTT
POGLUT-783Mut-seq-F	GTCCTAGTCCTGCTCACCTT
POGLUT1-5' arm-F	tgcttgtcgacGAAAAGACCATGAAGGGAGC
POGLUT1-3' arm-R	tcgagtgcggccgcacAACATTTGGAACTGTTAGTATTCTCTC
POGLUT1-5' arm-R	gtctaggaattcttgaatataacttcgtataatgtatgctatacgaagttatGTTCATGGAACTTTCTTTACATTCACC
POGLUT1-3' arm-F	tatcacgaattcaaacatataacttcgtatagcatacattatacgaagttatCAGCATTAGCATATATGTAAATTCTCC
POGLUT1-SUR-F1	CTCACCTTTCAGGGATTGGGAA
POGLUT1-SUR-R1	AGAGTGGACTGTAAACCAACGG

Table 1 Primer Sequences Used for Generation of Targeting Construct: Primers were generated using VectorNTI analysis for optimal primer sites and amplification of target sequence. Same primer sets, such as 5' and 3' primer sets as well as SUR primers were used for verification of correct insertion and verification of loxP removal.

2.5 In Vitro Differentiation of CTL, PT, and PTC iPSCs to Skeletal Muscle

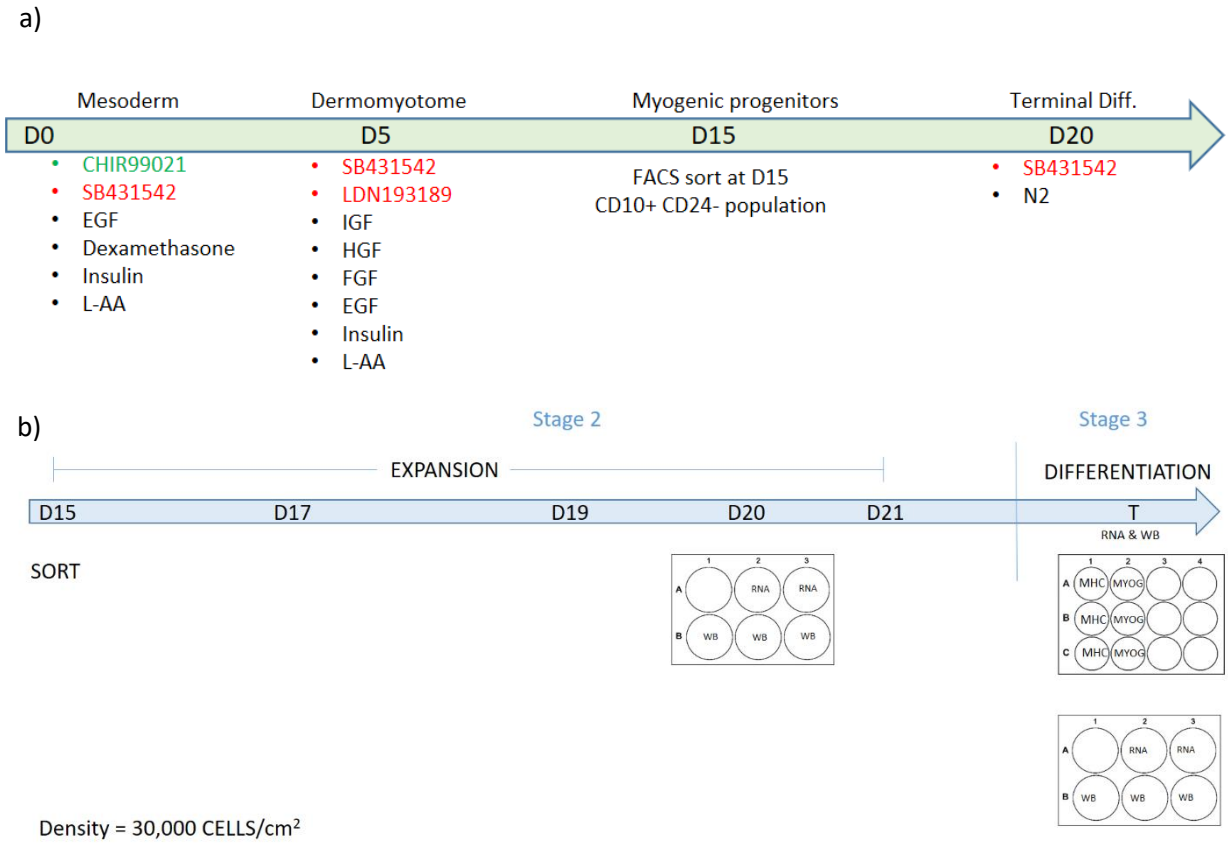

Figure 4 Myogenic differentiation of CTL, PT, and PTC iPSCs: a) Involves 5 day induction of mesoderm with a Wnt activator and TGF- β inhibitor followed by 10 days of selection for dermomyotome specification with TGF- β inhibitor and inhibition of BMP. b) Plans for expansion and sample harvesting after Day 15. Terminal differentiation involves staining for MHC and Myogenin for each cell line.

Previously published protocol as seen detailed in Figure 4 (Wu, et al., 2018) by our laboratory involves skeletal muscle differentiation in three stages. Reprogrammed iPSCs CTL, PT, and PTC were harvested using ACCUTASE™ cell detachment solution (Stem Cell Technologies, Catalog #07920), and seeded onto Corning Matrigel (Catalog #356234) coated plates at 30,000 cells/cm^2 in MDM-I and maintained for 5 days. MDM-I contained IMDM (Gibco, Catalog #12440053), 5% HS (Gibco, Catalog #26050088), 3 μM CHIR99021 (Selleck Chemical LLC, Catalog #S1263), 3 μM SB431542 (Selleck Chemical LLC, Catalog #S1067), 10 ng/ml hr-EGF (PeproTech Inc, Catalog #100-47), 10 μg/ml insulin (Millipore Sigma, Catalog #I9278), 0.4 mg/ml dexamethasone (Millipore Sigma, Catalog #D4902) and 200 μM L-ascorbic acid (Millipore Sigma, Catalog #A4403). Following 5 days of MDM-I, cells were harvested using ACCUTASE™ cell detachment solution (Stem Cell Technologies, Catalog #07920), and seeded onto Corning Matrigel (Catalog #356234) coated plates at 30,000 cells/cm^2 in MDM-II. MDM-II contained IMDM (Gibco, Catalog #12440053), 5% HS (Gibco, Catalog #26050088), 3 μM SB431542 (Selleck Chemical LLC, Catalog #S1067), 0.5 μM LDN193189 (Stemgent, Catalog #04-0074-10), 10 ng/ml hr-EGF (PeproTech Inc, Catalog #100-47), 10ng/ml hr-FGF (Pepro Tech Inc, Catalog #100-18B), 10ng/ml hr-IGF (Pepro Tech Inc, Catalog #350-10), 10ng/ml hr-HGF (Pepro Tech Inc, Catalog #100-139H), 10 μg/ml insulin (Millipore Sigma, Catalog #I9278), and 200 μM L-ascorbic acid (Millipore Sigma, Catalog #A4403). Cells were cultured until Day 15 on differentiation,

and then sorted using flow cytometry core with BD FacsAria II machine for $CD10^+$ $CD24^-$ population to enrich for myogenic progenitors (Wu, et al., 2018). Plan for harvesting of samples for RNA and western blot as well as differentiation and immunostaining shown in Figure 4 bottom image. Sorted cells were then plated on Corning Matrigel (Catalog #356234) coated plates at 30,000 cells/cm^2 in MDM-II to expand for terminal differentiation. Once cells reached full confluency media was switched to MDM-III. MDM-III contained: DMEM/F12 with GlutaMAX™ (Gibco, Catalog#10565018), 1% CTS N-2 Supplement (Gibco, Catalog #A1370701), 100 µM SB431542 (Selleck Chemical LLC, Catalog #S1067) (Hicks, et al., 2018). Cells were allowed to differentiate for 3 days then fixed for immunostaining.

2.6 Gene Expression Analysis of Differentiation

During time-course of differentiation, samples were seeded onto 6-well plates, 2 wells of which were used for RNA samples. Cells were directly lysed with TRIzol reagent (Invitrogen, Catalog #15596026) and stored at -80°C. Takara PrimeScript™ 1st strand cDNA Synthesis Kit was used to generate cDNA as per kit instructions (Clontech, Catalog #6110B). cDNA quality was verified by 3% agarose gel electrophoresis for GAPDH (Table 1). qPCR analysis was done on three biological replicates of differentiation samples, with two experimental replicates per sample. TaqMan™ universal PCR master mix (Applied Biosystems, Catalog #4304437) was used to carry out qPCR with TaqMan™ Gene Expression Assay Probes for Myogenic and Notch related genes as well as housekeeping as shown in Table 2 below. Ct values analyzed using SDS 2.4 ABI software and Microsoft Excel.

Probe	ID#	Amplicon Length (bp)
GAPDH	Hs02786624_g1	157
POGLUT1	Hs00220308_m1	90
NOTCH1	Hs01062014_m1	80
NOTCH3	Hs00166432_m1	87
DLL1	Hs00194509_m1	74
HEY1	Hs00232618_m1	66
HES1	Hs00172878_m1	78
PAX3	Hs00240950_m1	145
PAX7	Hs00242962_m1	73
MYOD1	Hs00159528_m1	67
MYF5	Hs00929416_g1	114
MYH3	Hs01074230_m1	65

Table 2 Probes from Applied Biosystems Gene Expression Assays used in qPCR analysis of myogenic differentiation.

2.7 Immunofluorescence and Quantification of MHC and MYOG

Cells were allowed to differentiate in MDM-III and fixed with 4% PFA (4% w/v Paraformaldehyde (Acros Organics, Catalog #41678-5000) in dPBS/Modified solution (HyClone, Catalog #SH30028.02)) for 15 minutes at RT and then washed with PBS 3x, followed by 0.3% Triton X-100 (Promega, Catalog #H5142) for 30 minutes at RT. Next, a 3% BSA solution (3% w/v BSA (Fisher Bioreagents, Catalog #BP1600-100) in dPBS/Modified solution (HyClone, Catalog #SH30028.02)) for 1 hour at RT followed by overnight incubation with primary antibody diluted in 3% BSA solution (MHC Supernatant adult MF20 DSHB antibody Catalog #MF20, AB_2147781 at 1:20 dilution; MYOG BD monoclonal antibody Catalog #556358 at 1:200 dilution). Overnight antibody washed the next day 3x with PBS for 5 minutes each then incubated 1 hour RT with secondary antibody diluted 1:500 with PBS (MHC with Invitrogen Goat Anti-Mouse IgG Alexa Fluor® 555 Catalog #A28180; MYOG with Invitrogen Goat Anti-Mouse IgG Alexa Fluor® 488 Catalog #A11001). Cells washed with PBS and then incubated with DAPI solution (Millipore Sigma, Catalog #508741) for 10 minutes at RT. Following DAPI staining, cells washed 2x for 5 minutes each and then imaged for quantification of $MHC^+/DAPI^+$ cells and $MYOG^+/DAPI^+$ cells. 6 images/well/cell line/marker. Images processed using ImageJ.

2.8 POGLUT1 Western Blot Analysis of Notch and Effectors

Protein samples were sent to the laboratory of Dr. Hamed Jafar-Nejad for western blot analysis. As per the laboratories protocol: Total proteins were quantified

using Pierce BCA Protein Assay (Cat #23228) and bovine serum albumin was used as standard. Protein extracts (20 µg per well) were separated on a 12% SDS-PAGE mini-PROTEAN TGX Precast gel (Bio-Rad Cat# 456-1046) and transferred onto PVDF membranes (Bio-Rad Cat# 1620177). Membranes were blocked in 5% skim milk powder in TBS-T at room temperature for 1 hour. Primary antibodies were diluted in blocking buffer and incubated with the membrane overnight at 4^{o}. The antibodies used in this study are Notch1-ICD, 1:1000 (Cell signaling Cat# 4147), NOTCH2-ICD, 0.5 µg/ml (DHSB Cat#C651.6DbHN), HES1, 1;1000 (Cell Signaling Cat# 11988), and Tubulin, 1:2000 (Santa Cruz Biotechnology Catalog #sc-5274).

2.9 Statistical Analysis

All statistical data processed using Microsoft Excel functions including 2 tail T-test, Mean, Standard Deviation, and Standard Error. All graphs and tables were also made in Microsoft Excel.

Chapter 3: Results

3.1 Generation of Targeting Construct

When generating the targeting construct, the 3' POGLUT1 homology arm was removed from the pStartK construct to allow for ligation of the puromycin selection cassette from pcDNA3.1 into the pStartK construct. Restriction digest with Eag1 and EcoR1 removed the 3' homology arm from the construct, and gel electrophoresis confirmed presence of the 3' arm (Figure 5). Following removal of the 3' homology arm, the cut pK-Poglut1-5'arm construct was purified and quality verified by Thermo Scientific™ NanoDrop 2000 (A260/280 ratio: 1.96). Next, the removed puromycin selection cassette was ligated into the pK-poglut1-5'arm construct using NEB NEBuilder® HiFi DNA Assembly Kit and verified with restriction digest for RsrII (Figure 6). Digest showed expected band sizes of 1.1 kb, 1.5 kb, and 4.0 kb. Clone 1 was chosen to move forward with generation of the targeting construct. Following ligation of puromycin selection cassette from pcDNA3.1 into the pK-poglut1-5'arm unfinished construct, the 3' homology arm was ligated back into the construct using NEB NEBuilder® HiFi DNA Assembly Kit and verified with restriction digest for HindIII (Figure 7). Expected band sizes were observed and construct was purified for final Gateway® reaction into pWS-TK6 construct. Following Gateway® reaction, agarose gel electrophoresis verified the HindIII digest gave expected band sizes of 1.1, 1.5, 1.8, and 5.7 kb as seen in Figure 8. Proper digestion verified the targeting construct is ready to generate PTC cell line.

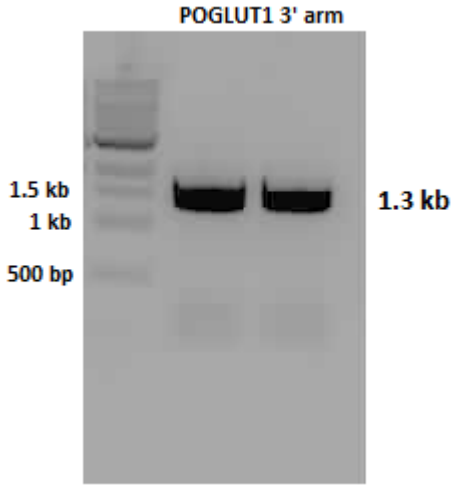

Figure 5 PCR Amplification of 3' POGLUT1 Homology Arm: PCR with 3'arm specific primer (Table 1) shows correct amplicon length of 1.3 kb and saved for later ligation back into the targeting construct prior to Gateway® reaction (both lanes are POGLUT1 3' arm)

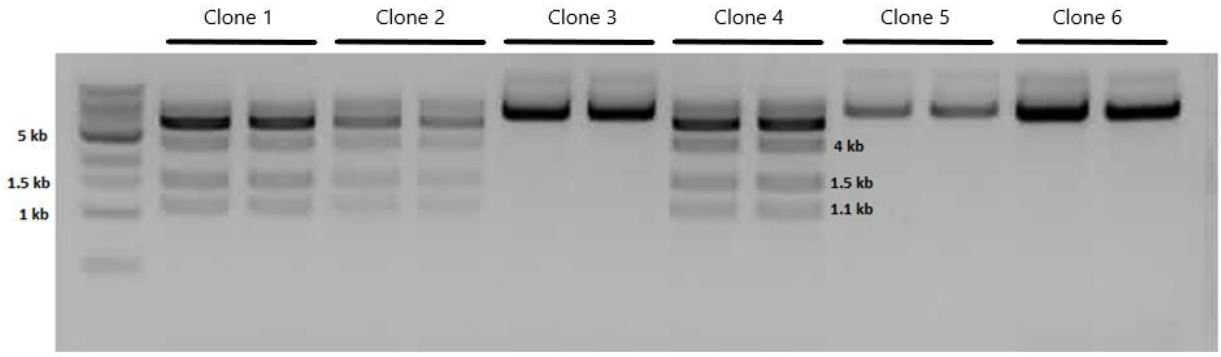

Figure 6 RsrII Digest of Partial Construct Clones 1-6: Digest with RsrII showing expected band sizes of 1.1, 1.5, and 4.0 kb. Clones 3, 5, and 6 are either negative or did not digest properly.

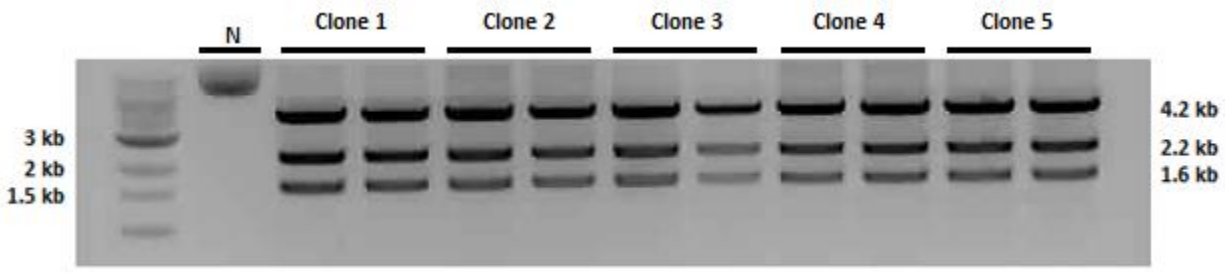

Figure 7 HindIII Digest of pK-Poglut1-Puro Construct: 5 clones were picked from Gibson assembly digest and verified for correct ligation and product sizes following digest. Expected band sizes are as follows: 1.6, 2.2, and 4.2 kb.

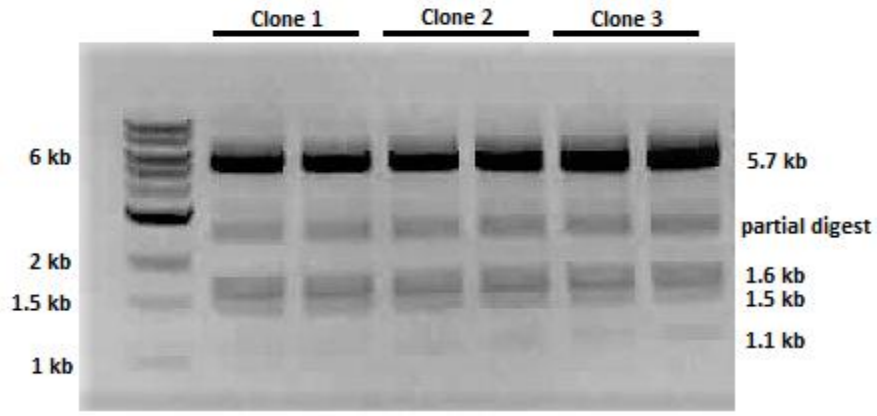

Figure 8 RsrII Digest of Final pWS-Poglut1-TK6-Puro Construct: RsrII digest on 1% agarose gel electrophoresis verifies expected band patterns of 1.1, 1.5, 1.8, and 5.7 kb.

3.2 Electroporation of pWS-Poglut1-TK6-Puro into PT II.5 and Expansion of Clones

Clones were observed prior to electroporation to ensure healthy and typical iPSC colonies are being used for electroporation (Figure 9). Following electroporation, cells were allowed to recover for 72 hours before starting puromycin treatment for selection. Figure 10 shows progression of cell recovery following electroporation to day 3, and then from the beginning of puromycin treatment for 7-10 days depending on when colonies were picked.

30 clones were picked and expanded, and 4 clones amplified positive for the 5' and 3' homology arm, two of which are shown in Figure 11 with expected band size of 1.7 kb versus no amplification in uncorrected PT II.5. Clones were then analyzed by DNA sequencing to verify correction of T>G mutation. Sequencing results indicate successful homologous recombination and correction in Clone 9 out of the four clones that showed positive for correct insertion. Figure 12 shows CTL, PT and PTC sequencing. Healthy control shows wild type thymine at c.699, however in PT the mutation changes to guanine, (T>G), changing the coding sequence from aspartic acid to glutamic acid (D233E). Sequencing of Clone 9 PTC indicates proper correction of mutation with reversal to guanine at c.699 (G>T). Prior to electroporation with pCAG-Cre-IRES2-GFP construct for removal of selection cassette, PTC Clone 9 was expanded to ensure proper iPSC morphology (Figure 13).

PTC Clone 9 was then electroporated with pCAG-Cre-IRES2-GFP construct for removal of puromycin selection cassette. Expansion of Cre recombinase treated clones

yielded dozens of clones of which 24 were picked for screening. Figure 14 shows expansion of clones in first four days of CloneR™ treatment.

Detection of successful removal of the selection cassette involved careful generation of a primer pair that spanned the length of the POGLUT1 genomic DNA to the single loxP site present after removal. If the primers did not amplify, this indicates the presence of the puromycin selection cassette. Indeed, the selection cassette was removed in 5 out of 7 clones screened and gave expected band sizes of 696 bp and 954 bp as shown in Figure 15.

Following verification and expansion for several passages of Cre-treated PTC Clone 9, iPSC pluripotency markers were stained to verify maintenance of pluripotency in the cell line. Indeed staining shown in Figure 16 shows consistent expression of pluripotency markers C-MYC, NANOG, OCT4a, SOX2, and KLF4.

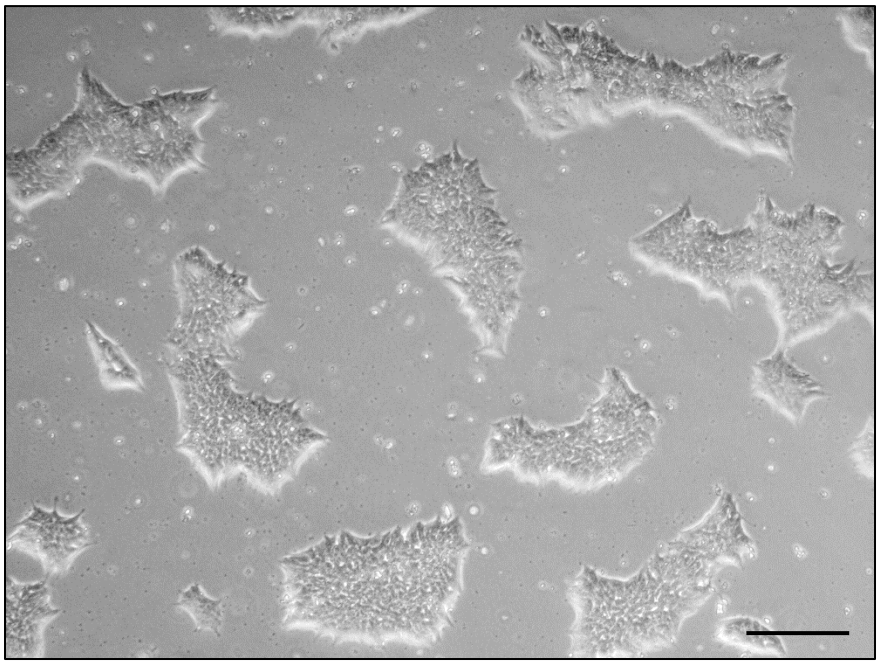

Figure 9 Morphology of PT II.5 iPSC: Morphology of PT II.5 prior to electroporation. Colony morphologies show typical iPSC shape, undifferentiated and healthy.

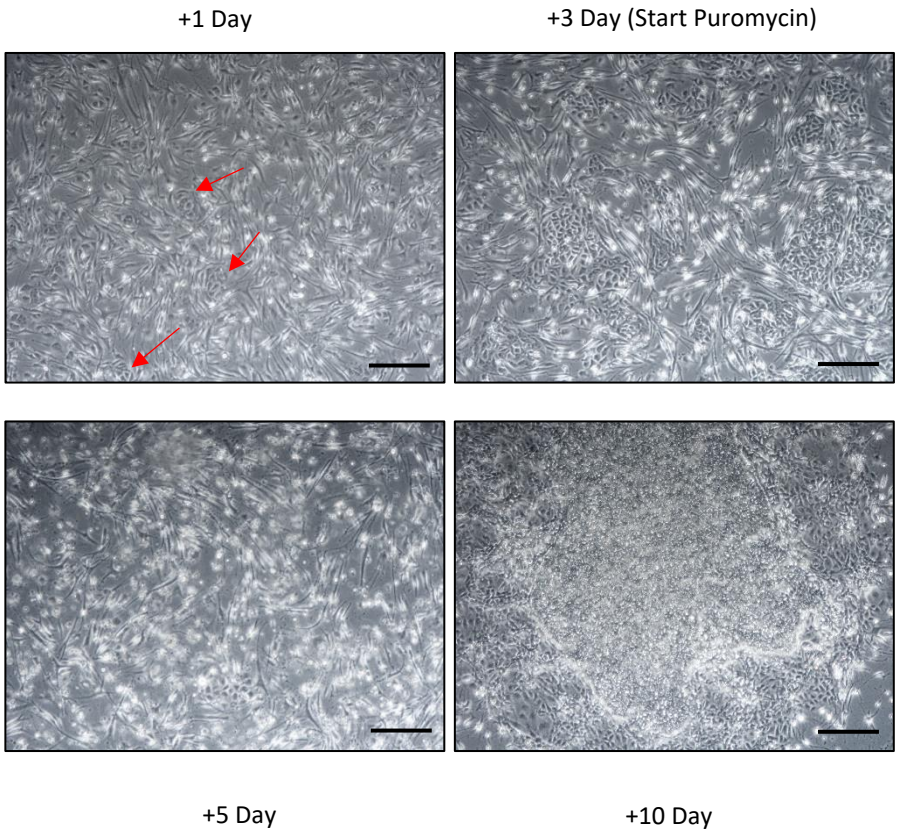

Figure 10 Recovery of Targeted PT II.5 from D0 - D10 Following Electroporation: Cells were recovered for 72 hours and then treated with puromycin for selection for 7-10 days until clones were picked. Single cell derived colonies indicated by red arrows. (4x magnification).

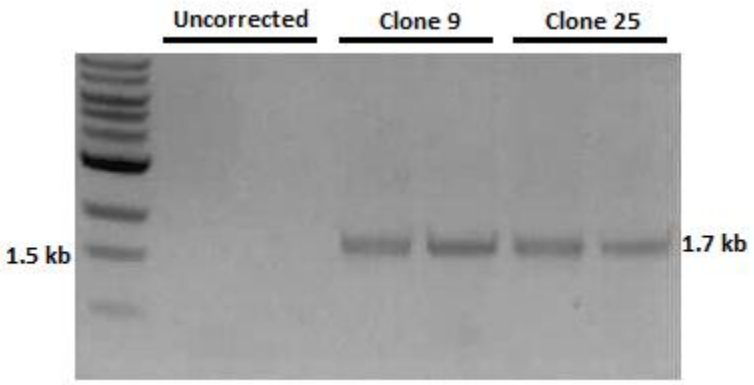

Figure 11 PCR of Uncorrected PT II.5 Versus clones 9 and 25: Expected band sizes for both the 5' and 3' arm are 1.7 kb.

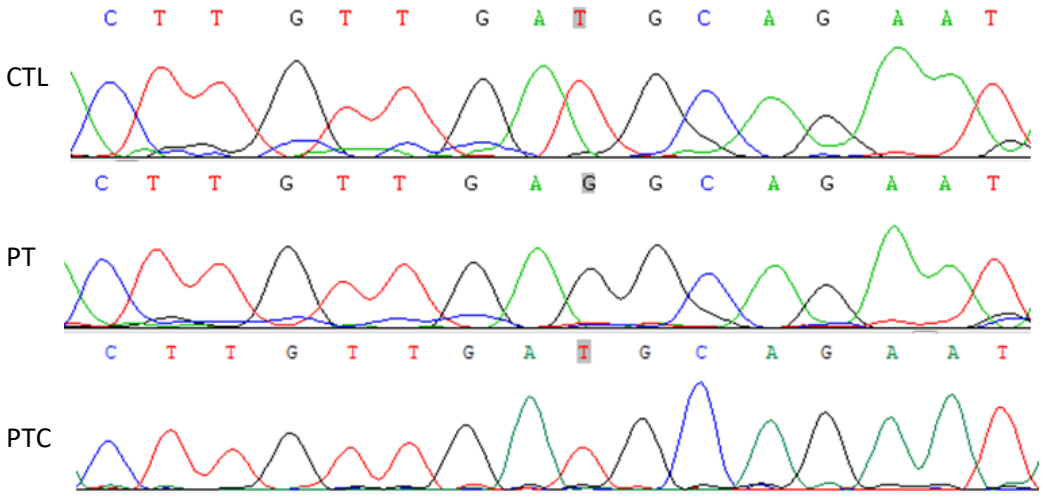

Figure 12 Sequencing results of CTL, PT, and PTC Clone 9: Sanger sequencing data indicates healthy control contains thymine at highlighted c.699, whereas PT II.5 indicates presence of T>G (thymine to glutamine) transversion missense mutation. This changes the protein translation of the codon from aspartic acid to glutamic acid (D233E). Clone 9

PTC sequencing confirms reversal of glutamic acid to aspartic acid at the indicated position and change back to original codon.

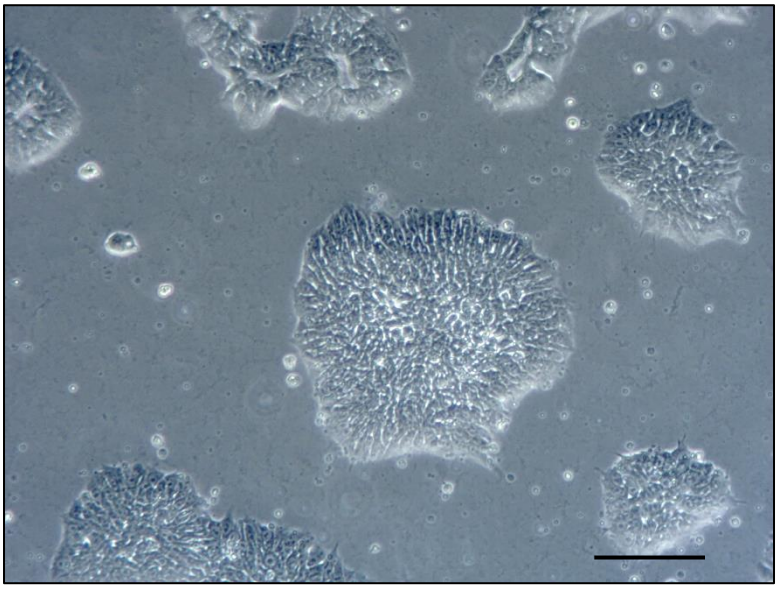

Figure 13 Morphology of iPSC PTC Clone 9: Morphology of clone shows round typical iPSC shape and lack of differentiated cells within culture (10x magnification).

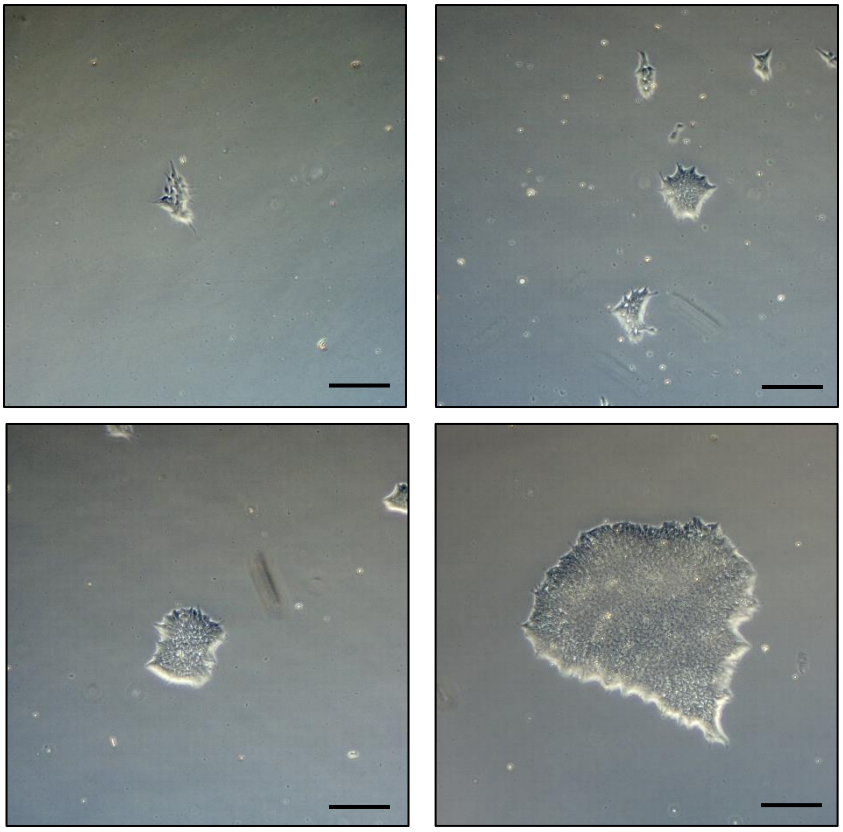

Figure 14 CloneR™ expanded cells after Cre recombinase: Following 4 days of CloneR™ expansion, PTC Clone 9 iPSCs revealed typical iPSC morphology and high survival. Cells were picked within 7-10 days. (4x magnification)

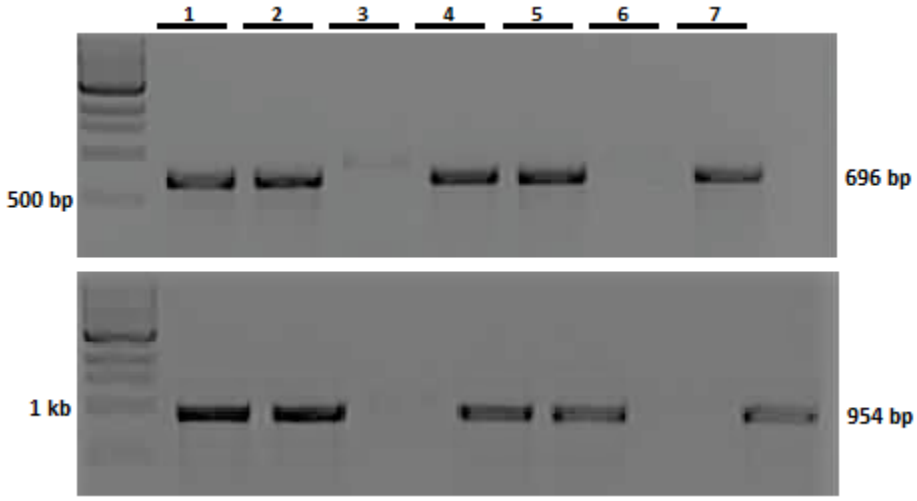

Figure 15 Gel electrophoresis of Cre Clones 1-7: Band sizes of PCR amplicons show expected sizes of from the 5' region (Top) and 3' region (bottom).

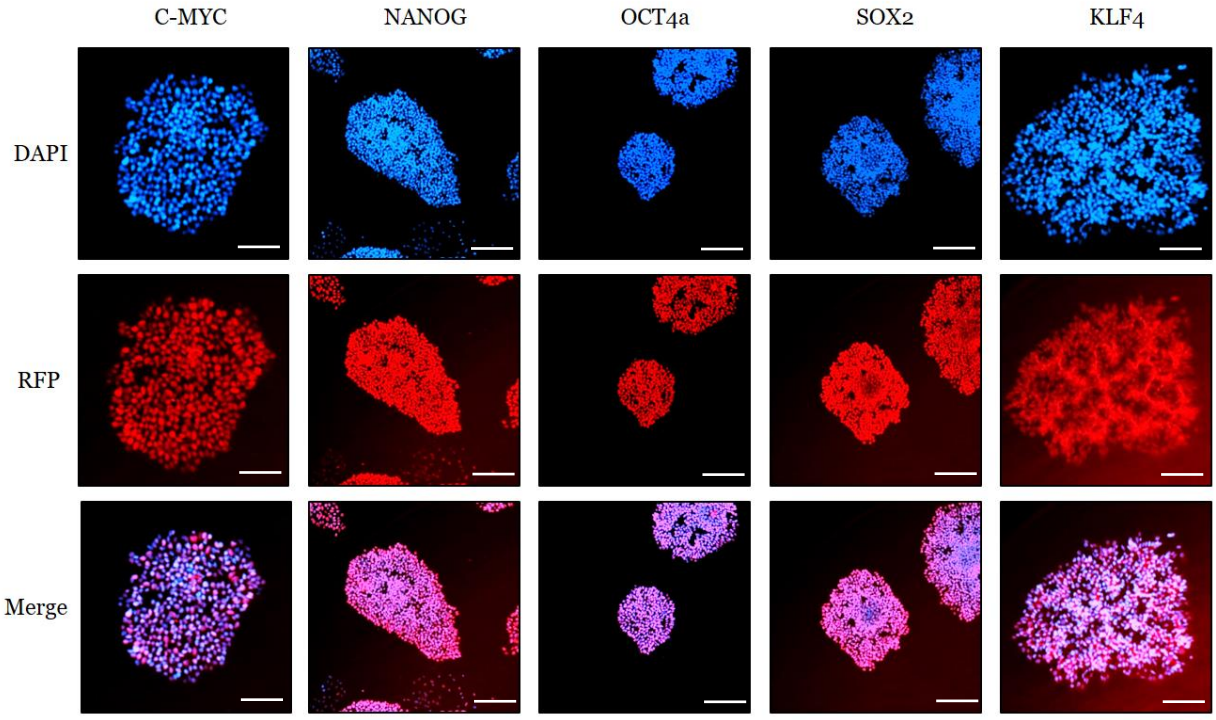

Figure 16 iPSC Pluripotency Marker Staining of Clone 9 PTC: Staining indicates proper expression of pluripotency markers C-MYC, NANOG, OCT4a, SOX2, and KLF4. (10x magnification)

3.3 In Vitro Differentiation of CTL, PT, and PTC iPSCs to Skeletal Muscle

Using a recently published protocol by our laboratory (Figure 4), CTL, PT and PTC cell lines were differentiated towards skeletal muscle lineage. During passage points and intermediate time points, cells were harvested and counted to assess proliferation. Indeed across the time points until Day 15, PTC cell line showed rescue of proliferation when compared to PT (Figure 19). At day 15, samples were harvested and prepared for sorting using $CD10^{+}$ $CD24^{-}$ cell surface markers previously discovered by our laboratory to mark a specific group of myogenic cells to enrich for myogenic differentiation potential (Wu et al. 2018) (Figure 17). In the evaluation of $CD10^{+}$ $CD24^{-}$ expression in myogenic progenitor cells, PTC exhibited higher expression of CD10 (a marker expressed on myogenic progenitors using this protocol) when compared to uncorrected PT cell line ($P<0.05$) (Figure 18). Once cells reached the point of terminal differentiation and fully confluent (Day 20), cells were switched to MDM-III and differentiated for three days and then fixed. Analysis of MHC^{+} and $MYOG^{+}$ myotubes showed statistically significant difference in MHC^{+} and $MYOG^{+}$ cells in PTC cells versus the uncorrected PT ($P<0.001$;$P<0.05$ respectively, Figures 20 and 21). Immunofluorescence image quantifications also confirmed a significant increase in MHC^{+} and $MYOG^{+}$ myofibers in PTC versus PT (Figures 22 and 23).

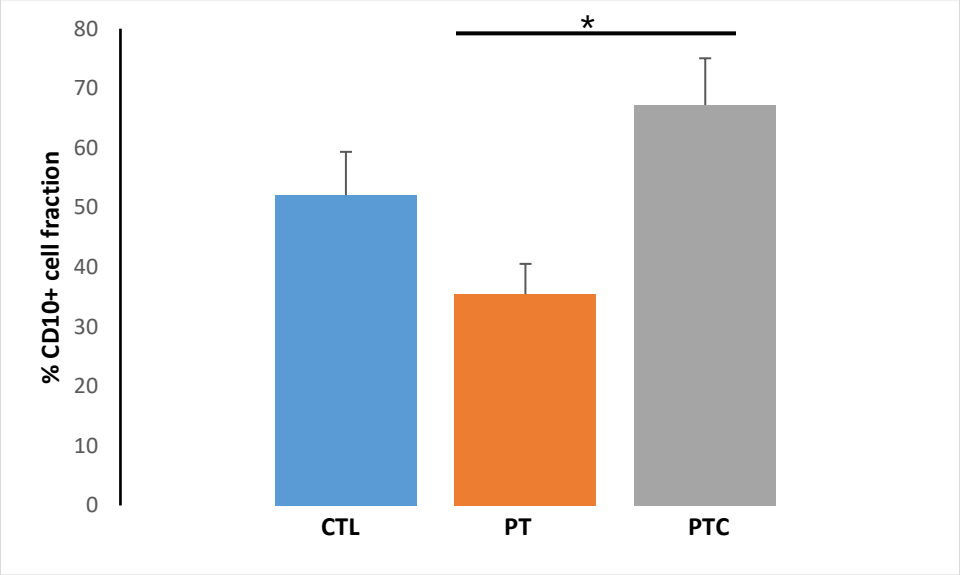

Figure 17 CD10^{+} Percentage of Expression in Sorted Cell Populations: In sorted cells, CD10^{+} expression across all 3 sample sets (marker of myogenic cells using this protocol) showed significantly higher myogenic population in corrected cells versus uncorrected ($P<0.05$).

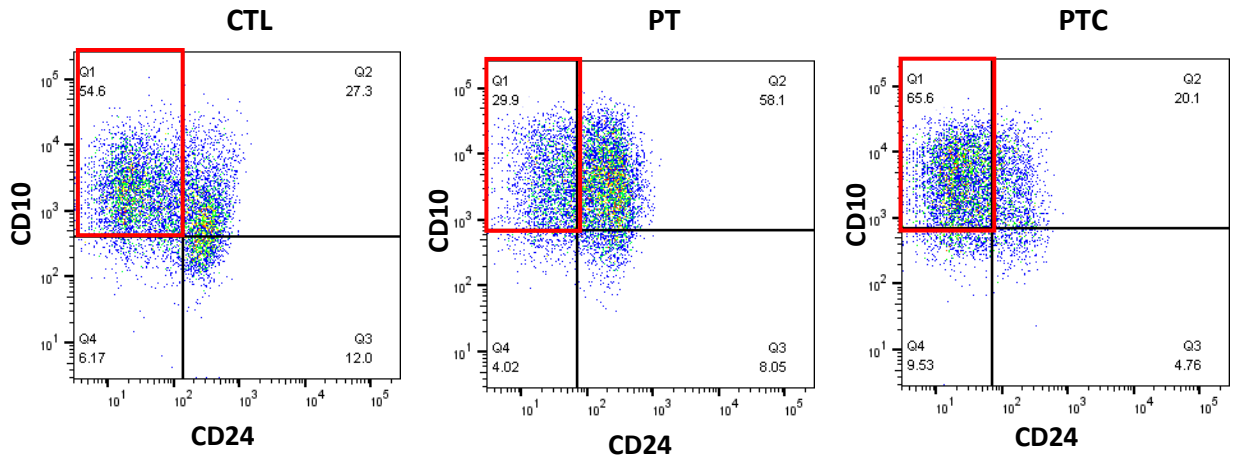

Figure 18 Gating of CD10^{+} CD24^{-} Cell Populations in Set 3 of Differentiation: Gating shows high percentage of myogenic cells in corrected (right) and control (left) versus uncorrected (center) cells.

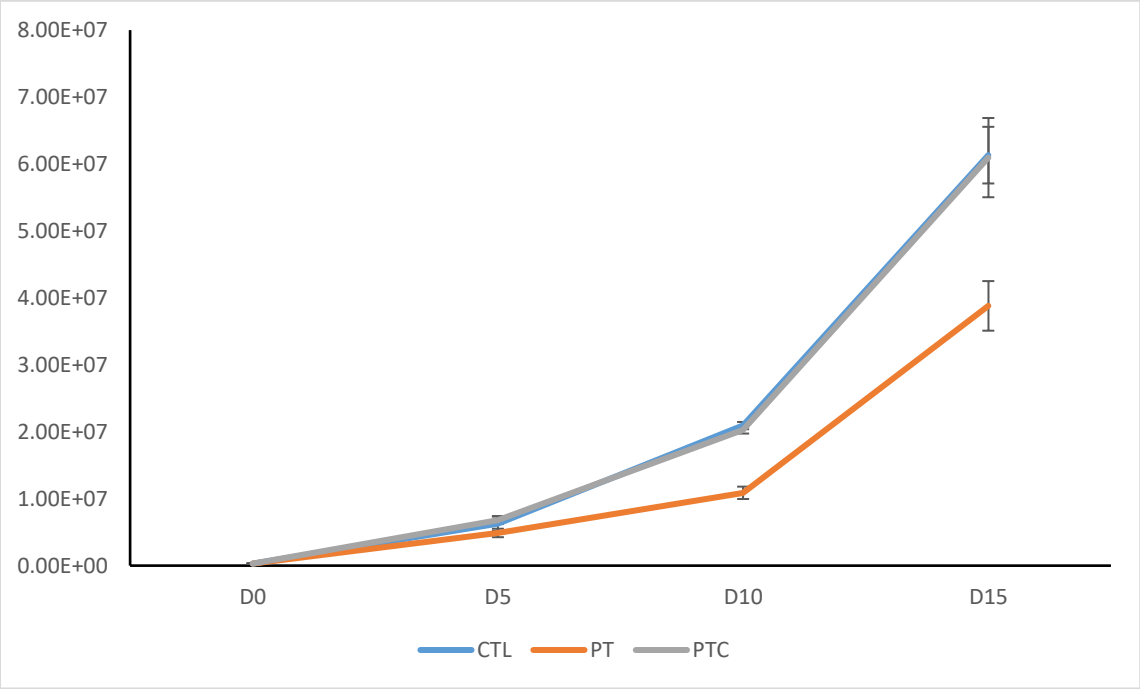

Figure 19 Proliferation curve showing growth of CTL, PT, and PTC cells during differentiation: Growth curves generated for time points Day 0, 5, 10, and 15 in each cell line.

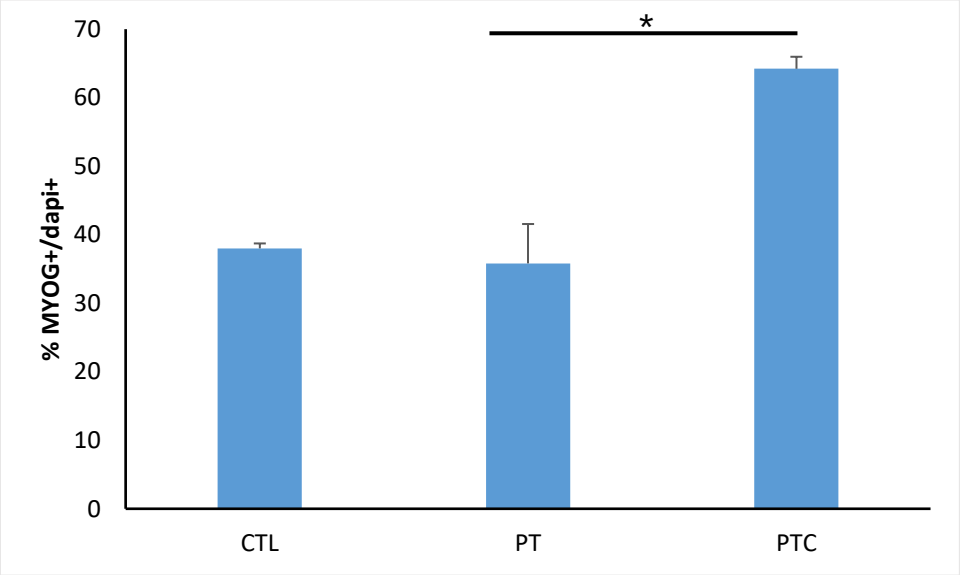

Figure 20 Percentage of MYOG$^+$ cells in myotubes: Quantification of MYOG$^+$ cells compared to total number of DAPI$^+$ cells in the field. Images quantified at 6 images/well. PTC compared to uncorrected PT shows statistically significant higher number of MYOG$^+$ cells ($P<0.05$).

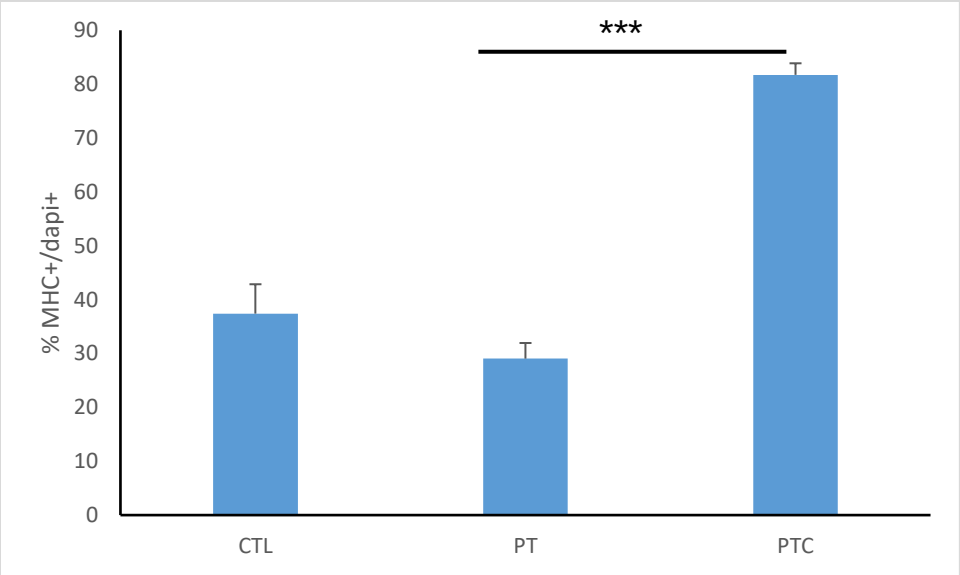

Figure 21 Percentage of MHC$^+$ cells in myotubes Quantification of MHC$^+$ cells compared to total number of DAPI$^+$ cells in the field. Images quantified at 6 images/well. PTC compared to uncorrected PT shows statistically significant higher number of MHC$^+$ cells (P<0.001).

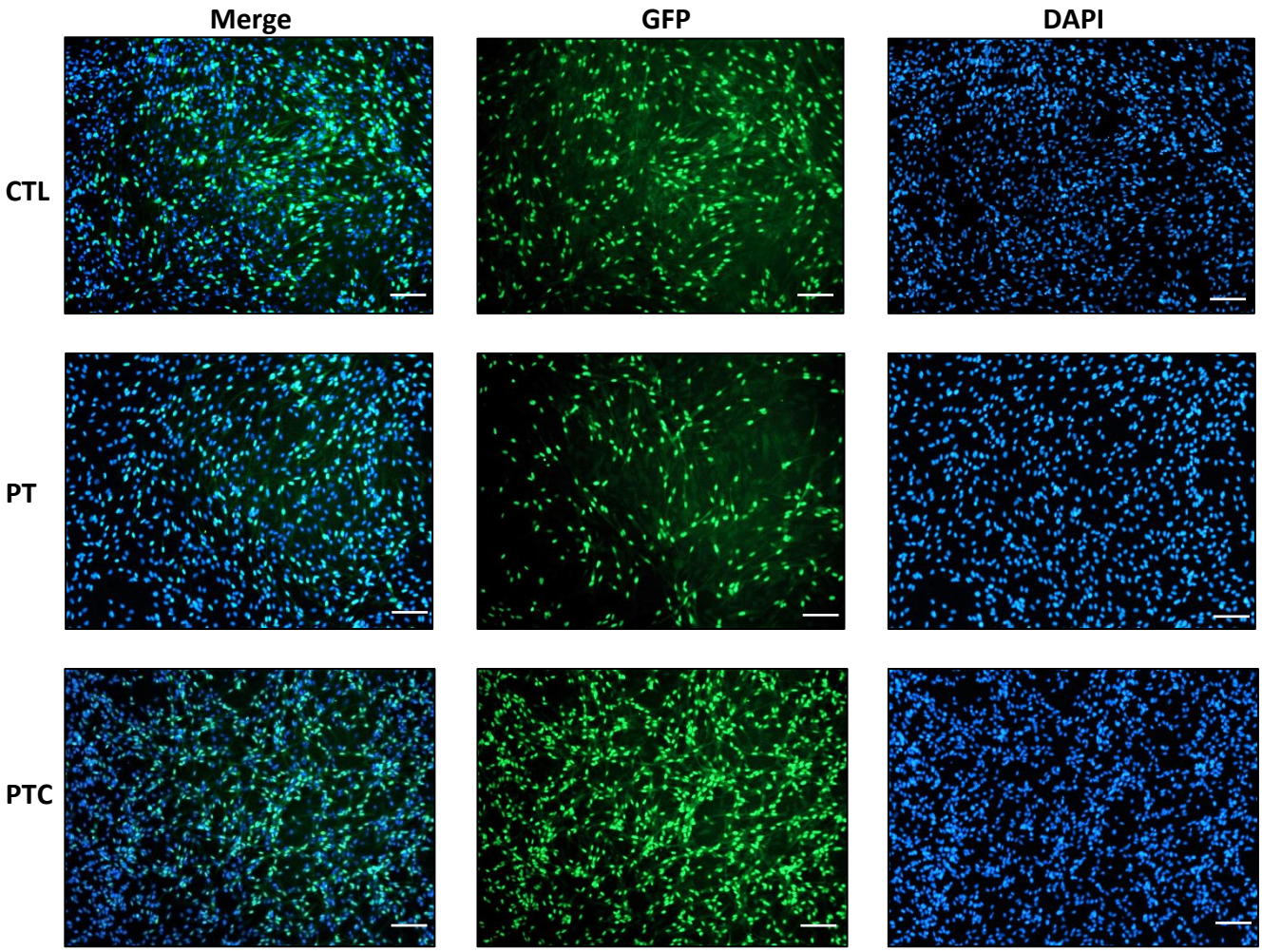

Figure 22 IFS imaging of CTL, PT, and PTC: IFS images show CTL (top row), PT (middle row), and PTC (bottom row) stained with MYOG and DAPI. Images clearly show

increased level of MYOG^{+} nuclei in fibers in the PTC cells versus PT after differentiation of the cells (MYOG in green, DAPI in blue).

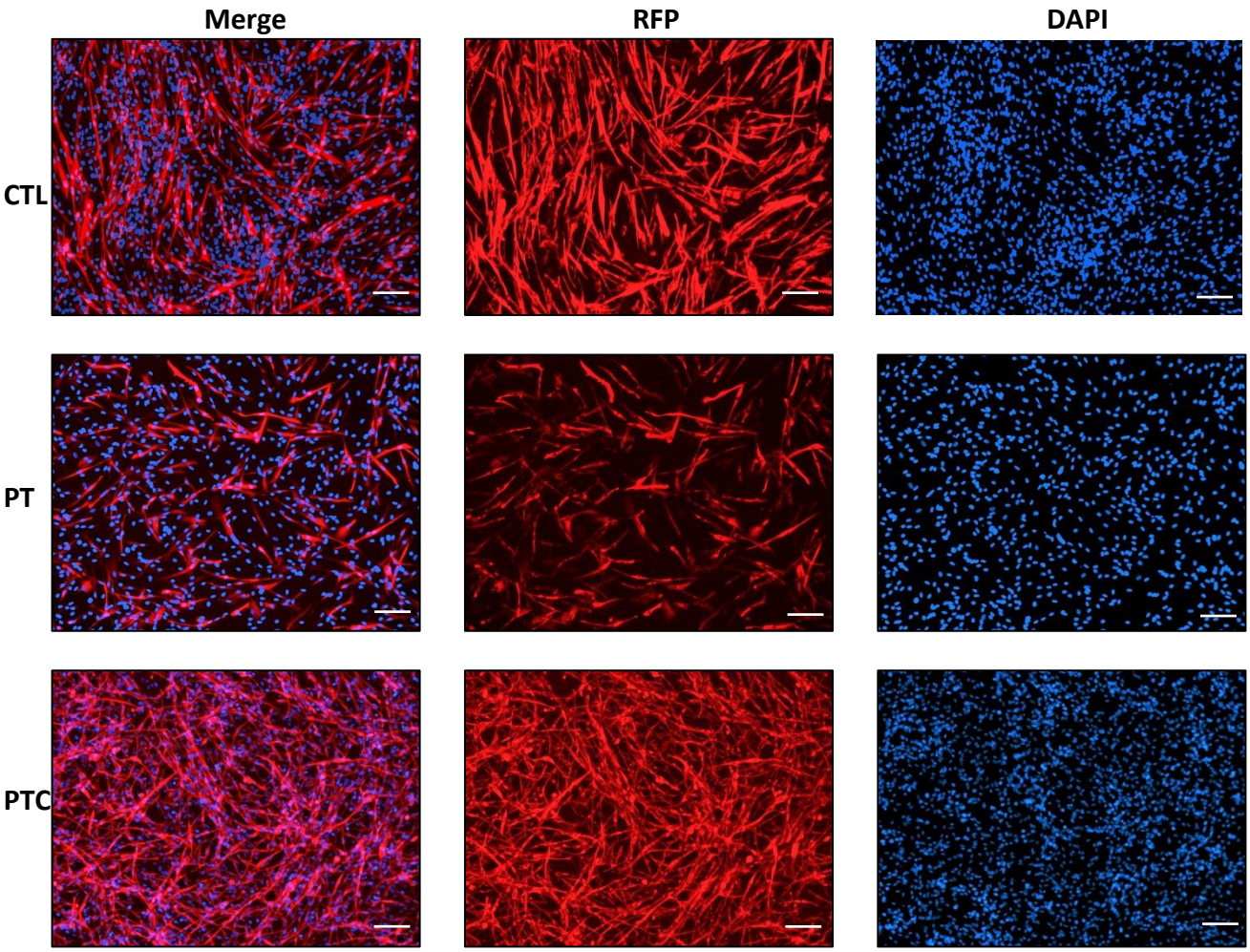

Figure 23 IFS imaging of CTL, PT, and PTC: IFS images show CTL (top row), PT (middle row), and PTC (bottom row) stained with MHC and DAPI. Images clearly show higher levels of percentage of MHC^{+} fibers, total amount of cells, as well as length and quality of the fibers in PTC vs PT cells (MHC in red, DAPI in blue).

3.3.1 Gene Expression Analysis of Notch and Myogenic Genes

Gene expression results of Notch related genes and Poglut1 showed higher expression in corrected cells in NOTCH1, HES1, HEY1, AND DLL1, while POGLUT1 and NOTCH3 are more or less consistently equal across time points or uncorrected cells are expressing higher than corrected, respectively. Myogenic genes showed higher levels of mRNA expression in uncorrected in MYF5, MYOD1, and PAX3, whereas MHC3 and PAX7 show higher levels of expression in corrected cells (Figures 24 and 25 respectively).

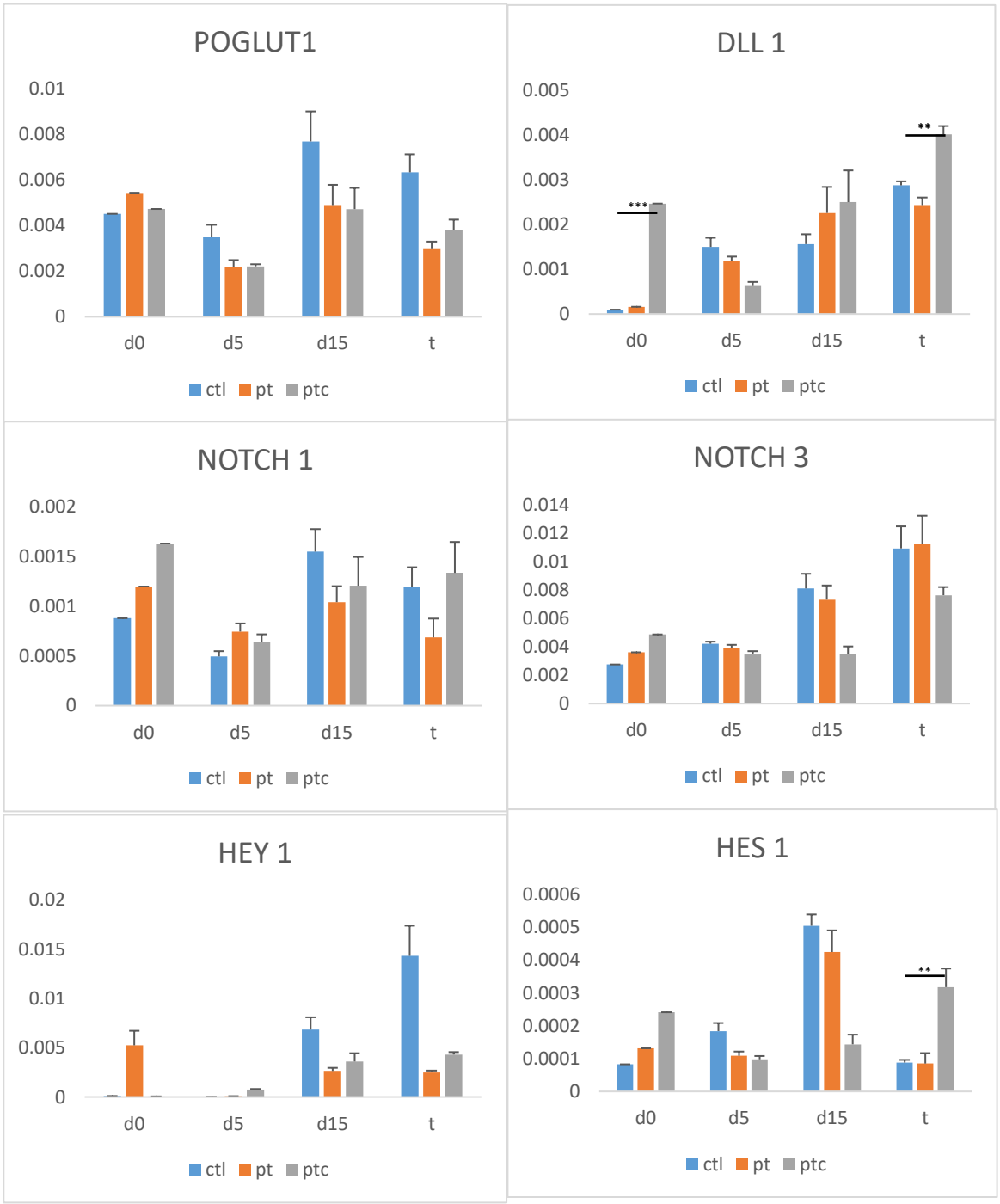

Figure 24 qPCR Analysis of POGLUT1 and Notch Signaling Genes: qPCR analysis involved major genes involved in the Notch pathway. Involved POGLUT1, NOTCH1, NOTCH3, ligand DLL1 (T;P<0.005), and downstream effectors HEY1 and HES1 (T; P<0.005).

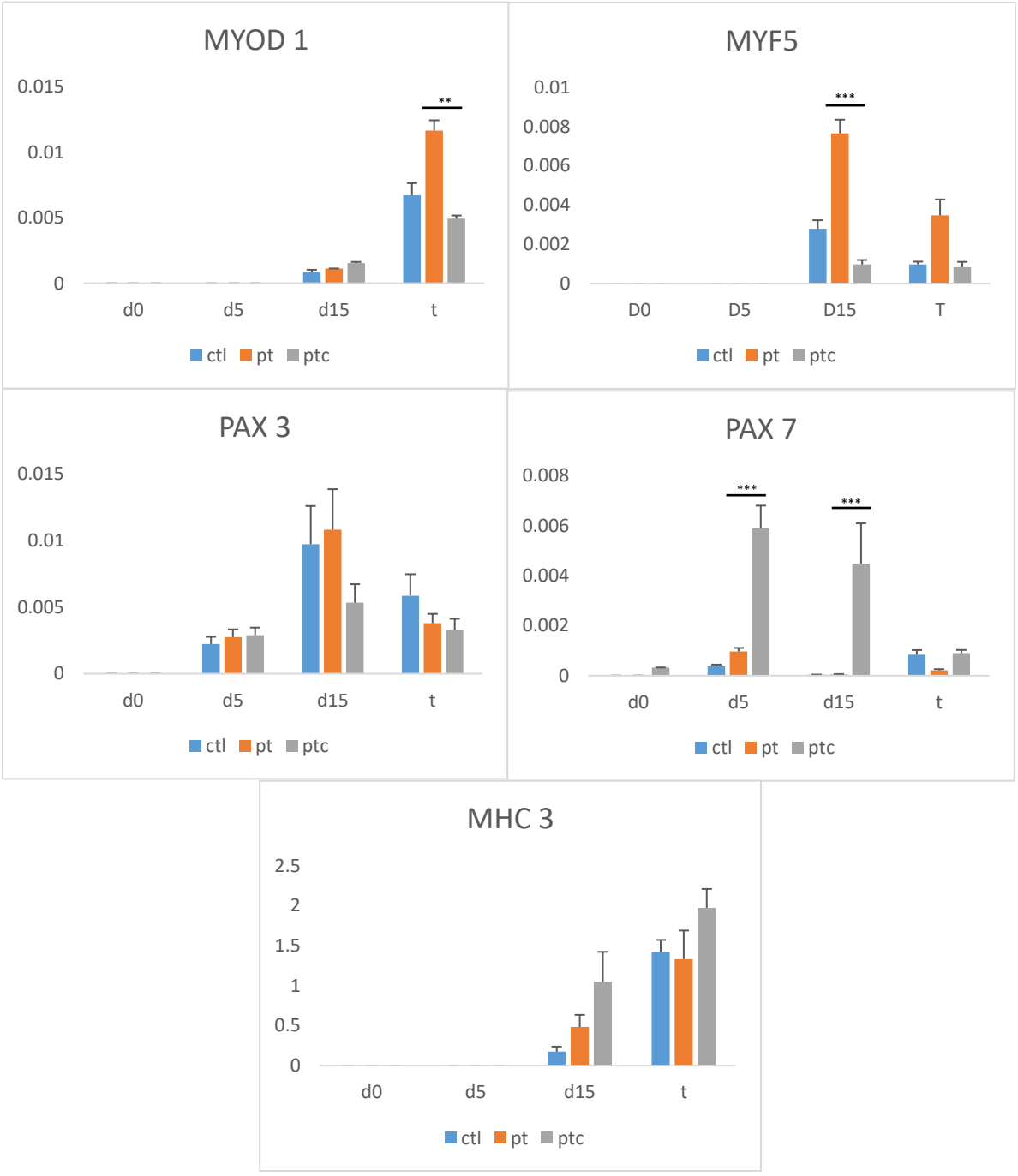

Figure 25 qPCR Analysis of Myogenic Signaling Genes: qPCR analysis involved major genes in the myogenic signaling pathway involving MYF5 (D15; $P<0.001$), MYOD1 (T; $P<0.05$), MHC, PAX3 and PAX7 (D5; $P<0.001$, D15; $P<0.001$).

3.3.2 Protein Analysis of Notch Intracellular Domains and Effector Hes1

Western Blot analysis shows N1ICD and N2ICD showed rescue in corrected cells versus uncorrected. Likewise, there is a significant level of recovery in the presence of downstream effector of Notch, Hes1 in corrected versus uncorrected cells. Tubulin samples indicated consistent and similar levels of expression confirming the quality of the protein samples (Figure 30).

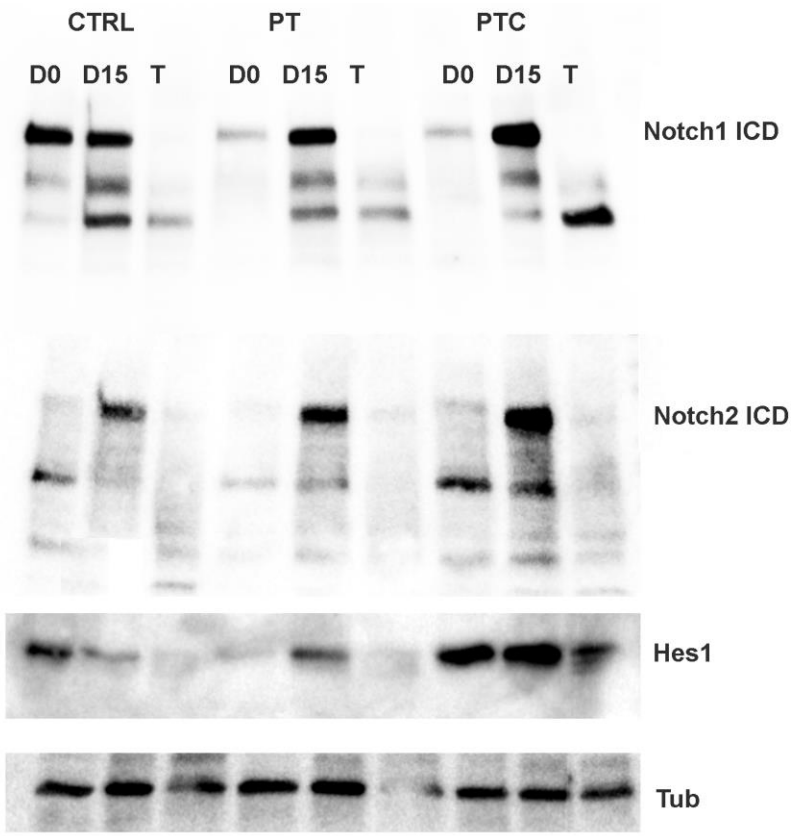

Figure 30 Western Blot of Notch Signaling Proteins: Western blot samples prepared by Dr. Nima Niknejad from the lab of Dr. Hamed Jafar-Nejad. N1ICD, N2ICD, and downstream effector Hes1 shown along with positive control Tubulin. Protein expression seen in NICD seem to be increased in PTC cells compared to PT, and downstream effector seems present in PTC but not in PT indicating rescue of downstream Notch signaling.

Chapter 4 Discussion

CRISPR/Cas9 based gene editing in muscle disorders provides promising technology in conjunction with patient-derived iPSCs for disease modeling and development of treatment for rare diseases. Currently there is no cure for muscular dystrophies and therapy consists of steroids, physical and surgical therapies for increasing range of motion, and management of disease related symptoms that often result in death (Mah, 2016). There are currently many therapies being developed ranging from use of iPSCs for disease modeling, drug screening to evaluate affected pathways and possible drug targets, and gene correction methods to look at global rescue of either full or partial muscle function (Ortiz-Vitali, 2019).

In this study, we aimed to generate a CRISPR/Cas9n based gene targeting construct to correct a homozygous recessive missense point mutation in a patient-derived cell line with a novel form of muscular dystrophy named LGMD2Z. Unlike DMD where the dystrophin gene is far too large, and mutations are far too variable, for a full gene targeting strategy, the presence of a single point mutation allows for use of this technology to study this novel LGMD. The Cas9 wild type nuclease system is a popular choice for engineering eukaryotic cells carrying specific mutations to drive NHEJ and HDR, however we utilized the Cas9 D10A mutant which contains a mutation in the catalytic RuvC domain which drives the DSB. This mutation allows for the Cas9 to generate a single-strand break as opposed to DSB, and targeting using a pair of Cas9n allows for carrying out gene editing with higher sequence specificity to reduce chance of off-target mutagenesis (Ran, et al., 2013). This involves two offset gRNA pairs to nick both strands of the locus to drive HDR, leading to advantages such as ease of customization, less off target effects and more specificity, higher editing efficiencies (Ran, et al., 2013). An alternative targeting method

was also tested using a single-strand oligonucleotide with wild-type Cas9 to generate DSB and correct the point mutation (Igoucheva, Alexeev, & Yoon, 2001). However after multiple attempts, this method was not successful and therefore we moved forward with the conventionally corrected PTC Clone 9 for differentiation. In the future, to generate higher efficiency of gene targeting, we will have to adjust our current strategy for targeting to find the optimal concentrations of targeting construct and sgRNA Cas9n constructs to increase correction percentage.

Using the patient-derived iPSCs, we also aimed to evaluate any rescue of phenotype in the corrected versus uncorrected and control cell lines. Currently, there is no established and widely accepted protocol for differentiation of hESCs or iPSCs to skeletal muscle. To give and idea of how many protocols currently exist (not counting this developed after the publication date, or those missed by the authors) Chal et al. compiled a list of many directed differentiation protocols in 2017 in chronological order from 1992-2017. At the time of publication, there were 81 total cited protocols. Differences between protocols included the type of format used, such as embryoid body or adherent cells, whether or not serum was used, the pathways involved, and if sorting was involved (Chal & Pourquié, 2017). Fortunately, by using a novel double-reporter hESC line, our lab has recently established a more efficient myogenic differentiation protocol for hPSCs (Wu et al. 2018). Using this directed differentiation protocol we seek to recapitulate, in stage 1 (MDM-1), the development of mesodermal progenitor cells by activation of Wnt signaling (von Maltzahn, Chang, Bentzinger, & Rudnicki, 2012) through inhibition of GSK-3 using the small molecule CHIR 99021. This small molecule is used in conjunction with a TGF-β inhibitor SB431542 (Inman, et al., 2002) since TGF-β is shown to repress

myogenesis by Smad3 (Liu, Black, & Derynck, 2001). From day 5 onward to sorting at day 15, the cells undergo further specification towards myogenic precursor cells in stage 2 (MDM-II) recapitulating primary myogenesis with activation of early myogenic genes such as PAX3 and PAX7, and later MYF5, MYOD, and lastly MHC when cells reach full commitment after expansion and terminal differentiation (D5-D25). To enrich for myogenic progenitor cells, our lab has discovered a unique set of cell surface markers ($CD10^+$ $CD24^-$) by using PAX7 and MYF5 double-reporter cell line that identifies a population of myogenic progenitor cells (Wu et al. 2018). Using this set of surface markers, we saw clear difference in percentage of $CD10^+$ (myogenic) cells in the corrected cells compared to the uncorrected cells. Coinciding with an increase in population of myogenic cells by D15, overall proliferation of corrected versus uncorrected cells showed significant improvement and rescue as demonstrated in Figure 19. This is further confirmed with a significantly lower percentage of myogenic cells ($MYOG^+$) cells during at terminal differentiation in uncorrected cells (Figure 20). In the discovery of the family containing the homozygous missense mutation in POGLUT1, Servián-Morilla et al. claim that lack of Notch signaling leads to loss of the $Pax7^+$ quiescence satellite cell pool which is responsible for muscle regeneration and maintenance of the stem cells of the muscle. This dysregulation is said to lead to seemingly accelerated differentiation which ultimately depletes the satellite cell pool sometime in late adulthood (Servián-Morilla, et al., 2016). Interestingly, we observed significantly less ($p<0.001$) MHC expression (i.e.myogenic cells) in uncorrected cells versus corrected, which indicates defective expansion ability of uncorrected myogenic cells probably due to dysregulated Notch signaling and faster cell

cycle exit.. While this does not completely support the hypothesis that patient cells experience accelerated differentiation, it is likely that during late stage 2 of differentiation (following sorting for enrichment of myogenic progenitors), cells within the population may be differentiating early and dying soon thereafter, due to the lack of the environment to support terminally differentiated cells (MDM-II is meant for expansion of progenitor cells and not terminal differentiation). It is also important to note that the cells used to make the claim that accelerated differentiation is observed in patient-derived cells comes from primary myoblasts. It is possible that due to the increased myogenic capacity of directly harvested and committed myoblasts, which might be in their late differentiation stage, while iPSC-derived cells more recapitulate developmental stages of myogenesis.

Following differentiation of iPSCs to skeletal myogenic progenitors, we evaluated the gene expression profile of three separate differentiation experiments in all three cell lines (CTL, PT, and PTC). To get a look at temporal gene expression, we evaluated specific time points during the process to get an idea what myogenic and notch signaling genes looked like at important events during our differentiation protocol. We began with Day 0 to get a look at the state of the iPSCs prior to beginning differentiation. D5 cells mark the beginning of committed muscle progenitor cells, and Day 15 is the point at which we sort the cells and further enrich the myogenic population. In the results, we labeled the terminal differentiation samples as T, which all represent the final day of differentiation in which samples were fixed for immunostaining, harvested for RNA samples as well as total protein for western blot. In all cell lines, POGLUT1 mRNA expression remained fairly consistent across all samples, and seemed to reach its highest expression at about D15. Notch 1 and 3 seem to have completely different results in uncorrected cells versus

corrected. Notch 1, which is responsible for maintenance of the Pax7^{+} satellite cell pool (with Notch2), and maintains cells in an undifferentiated quiescent state (Fujimaki et al. 2017) seems to be upregulated in corrected cells, whereas Notch 3, mostly found in vascular smooth muscle cells (Wang, Baron, & Trump, 2008) is higher in uncorrected cells. While higher expression of NOTCH1 would indicate some level of rescue in corrected cells, and correlate with the rescued DLL1 (which plays a role in maintain satellite cell pool during development (Sun et al. 2008), HEY1 and HES1 expression, it is possible that Notch 3 expression is being activated by DLL4 being expressed myogenic progenitor cells, or satellite cells, which is activating NOTCH3 and attempting to maintain the progenitor cell pool (Low et al. 2017). Currently, Notch signaling roles (canonically and non-canonically) are not well understood, and crosstalk plays a strong role in maintenance of satellite cell quiescence and activation. In the myogenic genes evaluated by qPCR, it appears that in the uncorrected cells, MYF5 and MYOD expression are higher than corrected cells. This supports the hypothesis that patient-derived cells experience accelerated differentiation, however interestingly MHC expression is higher in corrected cells. As mentioned before, it is possible that from Day 15 cells have begun to terminally differentiate spontaneously and die before reaching terminal differentiation. This is evident by the difference in total DAPI^{+} cells in the field of uncorrected cells versus healthy patient and corrected cells in Figures 20 and 21. Remarkably, overall levels of PAX7 in corrected cells were higher at each time point taken. Given that PAX7 is a major regulator of satellite cell quiescence and maintenance, it is likely that uncorrected cells are lacking mRNA expression due to dysregulated Notch signaling. While there are promising results in gene expression such as rescued Notch, and Notch effector and ligand, signaling, as

well as major quiescence regulator Pax7, it is important to also consider possible clonal variations -differentiation of iPSCs, as well as possible variations related to myogenic differentiation protocol. In addition, current 2-dimensional culture techniques appear to be lacking in replicating the true niche for formation of quiescent muscle stem cells, and it is likely that 3-dimensional or engineered scaffolds be a better option for this purpose.

Lastly, in western blot analysis of uncorrected and corrected cells, N1ICD and N2ICD as well as downstream effector HES1 protein levels were evaluated. There is clearly higher level of protein N2ICD (and possibly N1ICD) in corrected cells versus uncorrected. Given the role of Notch 2 in regulation of quiescence and regeneration, it appears that protein expression is rescued after correction, and there is higher level of Notch signaling taking place. This is also evident in the level of downstream effector Hes1, which is also rescued in corrected cells versus uncorrected. Given that N2ICD and Hes1, a major downstream effector of Notch signaling responsible for suppressing differentiation (Lahmann, et al., 2019) are rescued, it is clear that corrected cells have overall rescued Notch signaling, and supports our hypothesis that patient cells experienced reduced proliferation and decreased Notch signaling. More work is needed to evaluate if differentiation is truly accelerated or spontaneous. In the future, enzymatic and glycosylation studies of POGLUT1 enzyme from corrected and uncorrected cells are needed to evaluate the activity of POGLUT1 overall and towards glycosylation of EGF repeats in potential targets. Importantly, it would be also valuable to evaluate *in vivo* mice studies with patient corrected and uncorrected cells to determine the potential for myofiber engraftment and donor-derived satellite cell replenishment potential of the cells.

Chapter 5 Bibliography

Acar, M., Jafar-Nejad, H., Takeuchi, H., Rajan, A., Ibrani, D., Rana, N., . . . Bellen, H. (2008, 1 25). Rumi Is a CAP10 Domain Glycosyltransferase that Modifies Notch and Is Required for Notch Signaling. *Cell, 132*(2), 247-258.

Boldrin, L., Zammit, P., & Morgan, J. (2015, 1). Satellite cells from dystrophic muscle retain regenerative capacity. *Stem cell research, 14*(1), 20-29.

Brown, S., Torelli, S., Brockington, M., Yuva, Y., Jimenez, C., Feng, L., . . .Muntoni, F. (2004, 2). Abnormalities in alpha-dystroglycan expression in MDC1C and LGMD2I muscular dystrophies. *The American journal of pathology, 164*(2), 727-737.

Chal, J., & Pourquié, O. (2017, 6 15). Making muscle: skeletal myogenesis in vivo and in vitro. *Development, 144*(12), 2104.

Collins, C., Olsen, I., Zammit, P., Heslop, L., Petrie, A., Partridge, T., & Morgan, J. (2005, 7 29). Stem cell function, self-renewal, and behavioral heterogeneity of cells from the adult muscle satellite cell niche. *Cell, 122*(2), 289-301.

Cornelison, D., & Wold, B. (1997, 11 15). Single-Cell Analysis of Regulatory Gene Expression in Quiescent and Activated Mouse Skeletal Muscle Satellite Cells. *Developmental Biology, 191*(2), 270-283.

Cusella-De Angelis, M., Lyons, G., Sonnino, C., De Angelis, L., Vivarelli, E., Farmer, K., . . . Buckingham, M. (1992, 3 1). MyoD, myogenin independent differentiation of primordial myoblasts in mouse somites. *The Journal of cell biology, 116*(5), 1243-1255.

Ervasti, J., Ohlendieck, K., Kahl, S., Gaver, M., & Campbell, K. (1990). Deficiency of a glycoprotein component of the dystrophin complex in dystrophic muscle. *Nature, 345*(6273), 315-319.

Fernandez-Valdivia, R., Takeuchi, H., Samarghandi, A., Lopez, M., Leonardi, J., Haltiwanger, R., & Jafar-Nejad, H. (2011, 5). Regulation of mammalian Notch signaling and embryonic development by the protein O-glucosyltransferase Rumi. *Development (Cambridge, England), 138*(10), 1925-1934.

Galbiati, F., Volonté, D., Minetti, C., Bregman, D., & Lisanti, M. (2000, 12 1). Limb-girdle Muscular Dystrophy (LGMD-1C) Mutants of Caveolin-3 Undergo Ubiquitination and Proteasomal Degradation. *Journal of Biological Chemistry, 275*(48), 37702-37711.

Hicks, M., Hiserodt, J., Paras, K., Fujiwara, W., Eskin, A., Jan, M., . . . Pyle, A. (2018, 1). ERBB3 and NGFR mark a distinct skeletal muscle progenitor cell in human development and hPSCs. *Nature cell biology, 20*(1), 46-57.

Igoucheva, O., Alexeev, V., & Yoon, K. (2001). Targeted gene correction by small single-stranded oligonucleotides in mammalian cells. *Gene Therapy, 8*(5), 391-399.

Inman, G., Nicolás, F., Callahan, J., Harling, J., Gaster, L., Reith, A., . . . Hill, C. (2002, 7 1). SB-431542 Is a Potent and Specific Inhibitor of Transforming Growth Factor-β Superfamily Type I Activin Receptor-Like Kinase (ALK) Receptors ALK4, ALK5, and ALK7. *Molecular Pharmacology, 62*(1), 65.

Jiang, C., Wen, Y., Kuroda, K., Hannon, K., Rudnicki, M., & Kuang, S. (2014, 8). Notch signaling deficiency underlies age-dependent depletion of satellite cells in muscular dystrophy. *Disease models & mechanisms, 7*(8), 997-1004.

Kassar-Duchossoy, L. (2004). Mrf4 determines skeletal muscle identity in Myf5:Myod double-mutant mice. *Nature, 431*, 466-471.

Kitamoto, T. , and Hanaoka,K. (2010), Notch3 Null Mutation in Mice Causes Muscle Hyperplasia by Repetitive Muscle Regeneration. STEM CELLS, 28:2205-2216.

Koenig, M., Monaco, A., & Kunkel, L. (1988, 4 22). The complete sequence of dystrophin predicts a rod-shaped cytoskeletal protein. *Cell, 53*(2), 219-228.

Kopan, R., & Ilagan, M. (2009). The Canonical Notch Signaling Pathway: Unfolding the Activation Mechanism. *Cell, 137*(2), 216-233.

Kuang, S., Kuroda, K., Le Grand, F., & Rudnicki, M. (2007, 6 1). Asymmetric self-renewal and commitment of satellite stem cells in muscle. *Cell, 129*(5), 999-1010.

Lahmann, I., Bröhl, D., Zyrianova, T., Isomura, A., Czajkowski, M., Kapoor, V., . . . Birchmeier, C. (2019, 5 1). Oscillations of MyoD and Hes1 proteins regulate the maintenance of activated muscle stem cells. *Genes & Development, 33*(9-10), 524-535.

Le Grand, F., Jones, A., Seale, V., Scimè, A., & Rudnicki, M. (2009, 6 5). Wnt7a activates the planar cell polarity pathway to drive the symmetric expansion of satellite stem cells. *Cell stem cell, 4*(6), 535-547.

Lepper, C., Partridge, T., & Fan, C.-M. (2011, 9 1). An absolute requirement for Pax7-positive satellite cells in acute injury-induced skeletal muscle regeneration. *Development (Cambridge, England), 138*(17), 3639-3646.

Liu, D., Black, B., & Derynck, R. (2001, 11 15). TGF-beta inhibits muscle differentiation through functional repression of myogenic transcription factors by Smad3. *Genes & development, 15*(22), 2950-2966.

Low, S., Barnes, J., Zammit, P., & Beauchamp, J. (2018, 3 1). Delta-Like 4 Activates Notch 3 to Regulate Self-Renewal in Skeletal Muscle Stem Cells. *STEM CELLS, 36*(3), 458-466.

Mah, J. (2016, 7 22). Current and emerging treatment strategies for Duchenne muscular dystrophy. *Neuropsychiatric disease and treatment, 12*, 1795-1807.

Mahadevan, M., Tsilfidis, C., Sabourin, L., Shutler, G., Amemiya, C., Jansen, G., . . . et, a. (1992, 3 6). Myotonic dystrophy mutation: an unstable CTG repeat in the 3' untranslated region of the gene. *Science, 255*(5049), 1253.

MAURO, A. (1961). Satellite cell of skeletal muscle fibers. *The Journal of biophysical and biochemical cytology*.

Muchir, A., Bonne, G., van der Kooi, A., van Meegen, M., Baas, F., Bolhuis, P., . . . Schwartz, K. (2000, 5 22). Identification of mutations in the gene encoding lamins A/C in autosomal dominant limb girdle muscular dystrophy with atrioventricular conduction disturbances (LGMD1B). *Human Molecular Genetics, 9*(9), 1453-1459.

Noguchi, Y.-t., Nakamura, M., Hino, N., Nogami, J., Tsuji, S., Sato, T., . . . Fukada, S.-i. (2019, 2 15). Cell-autonomous and redundant roles of Hey1 and HeyL in muscle stem cells: HeyL requires Hes1 to bind diverse DNA sites. *Development, 146*(4), dev163618.

Parker, M., Loretz, C., Tyler, A., Duddy, W., Hall, J., Olwin, B., . . . Tapscott, S. (2012, 10). Activation of Notch signaling during ex vivo expansion maintains donor muscle cell engraftment. *Stem cells (Dayton, Ohio), 30*(10), 2212-2220.

Ran, F., Hsu, P., Wright, J., Agarwala, V., Scott, D., & Zhang, F. (2013, 10 24). Genome engineering using the CRISPR-Cas9 system. *Nature Protocols, 8*, 2281.

Rana, N., Nita-Lazar, A., Takeuchi, H., Kakuda, S., Luther, K., & Haltiwanger, R. (2011, 9 9). O-glucose trisaccharide is present at high but variable stoichiometry at multiple sites on mouse Notch1. *The Journal of biological chemistry, 286*(36), 31623-31637.

Rantanen,Hurme, T., Lukka, R., Heino, J., Kalimo, H. (1995). Satellite cell proliferation and the expression of myogenin and desmin in regenerating skeletal muscle: evidence for two different populations of satellite cells. *Laboratory Investigations, 72*(3), 341-347.

Relaix, F., Montarras, D., Zaffran, S., Gayraud-Morel, B., Rocancourt, D., Tajbakhsh, S., . . . Buckingham, M. (2006). Pax3 and Pax7 have distinct and overlapping functions in adult muscle progenitor cells. *Journal of Cell Biology*.

Sambasivan, R., Yao, R., Kissenpfennig, A., Van Wittenberghe, L., Paldi, A., Gayraud-Morel, B., . . . Galy, A. (2011, 10 1). Pax7-expressing satellite cells are

indispensable for adult skeletal muscle regeneration. *Development, 138*(19), 4333.

Schultz, E., Gibson,M.C., Champion, T. (1978). Satellite cells are mitotically quiescent in mature mouse muscle: an EM and radioautographic study. *Journal of Experimental Zoology, 206*(3), 451-456.

Servián-Morilla, E., Takeuchi, H., Lee, T., Clarimon, J., Mavillard, F., Area-Gómez, E., . . . Paradas, C. (2016, 10 10). A POGLUT1 mutation causes a muscular dystrophy with reduced Notch signaling and satellite cell loss. *EMBO molecular medicine, 8*(11), 1289-1309.

Shin Fujimaki Daiki Seko Yasuo Kitajima Kiyoshi Yoshioka Yoshifumi Tsuchiya Shinya Masuda Yusuke Ono. (2017). Notch1 and Notch2 Coordinately Regulate Stem Cell Function in the Quiescent and Activated States of Muscle Satellite Cells. *Stem Cells, 36*(2).

Sun, D., Li, H., & Zolkiewska, A. (2008, 11 15). The role of Delta-like 1 shedding in muscle cell self-renewal and differentiation. *Journal of cell science, 121*(Pt 22), 3815-382

Tawil, R., & Van Der Maarel, S. (2006, 7 1). Facioscapulohumeral muscular dystrophy. *Muscle & Nerve, 34*(1), 1-15.

TYLER, F., & STEPHENS, F. (1950, 4 1). STUDIES IN DISORDERS OF MUSCLE. II. CLINICAL MANIFESTATIONS AND INHERITANCE OF FACIOSCAPULOHUMERAL DYSTROPHY IN A LARGE FAMILY*. *Annals of Internal Medicine, 32*(4), 640-660.

von Maltzahn, J., Chang, N., Bentzinger, C., & Rudnicki, M. (2012, 11). Wnt signaling in myogenesis. *Trends in cell biology, 22*(11), 602-609.

Wang, T., Baron, M., & Trump, D. (2008). An overview of Notch3 function in vascular smooth muscle cells. *Progress in Biophysics and Molecular Biology, 96*(1), 499-509.

Wu, J., Hunt, S., Matthias, N., Servián-Morilla, E., Lo, J., Jafar-Nejad, H., . . . Darabi, R. (2017, 10). Generation of an induced pluripotent stem cell line (CSCRMi001-A) from a patient with a new type of limb-girdle muscular dystrophy (LGMD) due to a missense mutation in POGLUT1 (Rumi). *Stem cell research, 24*, 102-105.

Wu, J., Matthias, N., Lo, J., Ortiz-Vitali, J., Shieh, A., Wang, S., & Darabi, R. (2018, 11 13). A Myogenic Double-Reporter Human Pluripotent Stem Cell Line Allows Prospective Isolation of Skeletal Muscle Progenitors. *Cell reports, 25*(7), 1966-1981.e4.

Yoshida, M., & Ozawa, E. (1990, 11 1). Glycoprotein Complex Anchoring Dystrophin to Sarcolemma1. *The Journal of Biochemistry, 108*(5), 748-752.

Zammit, P., Golding, J., Nagata, Y., Hudon, V., Partridge, T., & Beauchamp, J. (2004). Muscle satellite cells adopt divergent fates: A mechanism for self-renewal? *Journal of Cell Biology*.

Zhao, P., & Hoffman, E. (2004). Embryonic Myogenesis Pathways in Muscle Regeneration. *Developmental Dynamics*.

VITA

Jose Ortiz-Vitali was born in Houston, Texas and raised in Deer Park, Texas. Before attending UT Health MD Anderson Cancer Center Graduate School of Biomedical Sciences, he attended Baylor University from 2011-2013, and subsequently The University of Houston – Clear Lake from 2014-2015 where he earned his Bachelor of Science Degree in Biological Sciences with a specialization in Biotechnology. His undergraduate research was conducted under the direction of Dr. Lory Santiago-Vazquez and involved a collaborative project with Lonza on evaluation of microbial induced corrosion of oil and gas pipelines. While at Baylor University, Jose was a member of Phi Iota Alpha Latino Fraternity Inc. where he developed leadership skills in executive board positions and led events such as a merit-based scholarship pageant which awarded women of Baylor University $5,000 in scholarship. At The University of Houston – Clear Lake, Jose was an early member of the Nu Xi Delta chapter of Beta Beta Beta Biological Honor Society and president. He was involved in celebrating the achievements of exceptionally gifted local high school students who won local science-fair events and were invited to the university to participate in lab tours, seminars, and presentations of their own science-fair projects. At GSBS, Jose was chosen by the Scientist Mentoring Diversity Program for a scholarship in which he was paired with a mentor from Amgen, attended BIO international biotechnology and pharmaceutical conference in San Diego, California, and established networking relationships. His thesis is under the guidance of Dr. Radbod Darabi.